Gasdermin E mediates photoreceptor damage by all-*trans*-retinal in the mouse retina

Received for publication, October 18, 2021, and in revised form, December 19, 2021 Published, Papers in Press, December 29, 2021,
https://doi.org/10.1016/j.jbc.2021.101553

Binxiang Cai[1], Chunyan Liao[1], Danxue He[1], Jingmeng Chen[2], Jiahuai Han[3], Jiaying Lu[1], Kaiqi Qin[1], Wenxu Liang[1], Xiaoling Wu[1], Zuguo Liu[1], and Yalin Wu[1,4,5,*]

From the [1]Fujian Provincial Key Laboratory of Ophthalmology and Visual Science, Department of Ophthalmology, Fujian Engineering and Research Center of Eye Regenerative Medicine, Xiang'an Hospital of Xiamen University, Eye Institute of Xiamen University, Xiamen City, Fujian, China; [2]School of Medicine, and [3]State Key Laboratory of Cellular Stress Biology, Innovation Center for Cell Biology, School of Life Sciences, Xiamen University, Xiamen City, Fujian, China; [4]Xiamen Eye Center of Xiamen University, School of Medicine, Xiamen University, Xiamen City, Fujian, China; [5]Shenzhen Research Institute of Xiamen University, Shenzhen City, Guangdong, China

Edited by Roger Colbran

The breakdown of all-*trans*-retinal (atRAL) clearance is closely associated with photoreceptor cell death in dry age-related macular degeneration (AMD) and autosomal recessive Stargardt's disease (STGD1), but its mechanisms remain elusive. Here, we demonstrate that activation of gasdermin E (GSDME) but not gasdermin D promotes atRAL-induced photoreceptor damage by activating pyroptosis and aggravating apoptosis through a mitochondria-mediated caspase-3-dependent signaling pathway. Activation of c-Jun *N*-terminal kinase was identified as one of the major causes of mitochondrial membrane rupture in atRAL-loaded photoreceptor cells, resulting in the release of cytochrome *c* from mitochondria to the cytosol, where it stimulated caspase-3 activation required for cleavage of GSDME. Aggregation of the N-terminal fragment of GSDME in the mitochondria revealed that GSDME was likely to penetrate mitochondrial membranes in photoreceptor cells after atRAL exposure. ABC (subfamily A, member 4) and all-*trans*-retinol dehydrogenase 8 are two key proteins responsible for clearing atRAL in the retina. *Abca4*$^{-/-}$*Rdh8*$^{-/-}$ mice exhibit serious defects in atRAL clearance upon light exposure and serve as an acute model for dry AMD and STGD1. We found that N-terminal fragment of GSDME was distinctly localized in the photoreceptor outer nuclear layer of light-exposed *Abca4*$^{-/-}$*Rdh8*$^{-/-}$ mice. Of note, degeneration and caspase-3 activation in photoreceptors were significantly alleviated in *Abca4*$^{-/-}$*Rdh8*$^{-/-}$*Gsdme*$^{-/-}$ mice after exposure to light. The results of this study indicate that GSDME is a common causative factor of photoreceptor pyroptosis and apoptosis arising from atRAL overload, suggesting that repressing GSDME may represent a potential treatment of photoreceptor atrophy in dry AMD and STGD1.

Vision is one of the most common and fundamental senses that enable the perception of the surrounding environment. The classical visual (retinoid) cycle is a long-known enzymatic pathway that converts all-*trans*-retinal (atRAL) to 11-*cis*-retinal in rod and cone photoreceptor outer segments (OSs) and the adjacent retinal pigment epithelium (RPE) for the regeneration of visual pigments (1–3). Compromised clearance of atRAL leads to an accumulation of atRAL in the cytosol of photoreceptor OSs, which has close relation with photoreceptor degeneration in dry age-related macular degeneration (AMD) and autosomal recessive Stargardt's disease 1 (STGD1) (4–7). A key function for both photoreceptor-specific ABC (subfamily A, member 4) transporter (ABCA4) and all-*trans*-retinol (atROL) dehydrogenase 8 (RDH8) is to satisfactorily eliminate free atRAL in the visual (retinoid) cycle (8–10). Mice with a genetic deletion of *Abca4* and *Rdh8* genes (*Abca4*$^{-/-}$*Rdh8*$^{-/-}$ mice) display defects in atRAL clearance and age-related photoreceptor atrophy (5). *Abca4*$^{-/-}$*Rdh8*$^{-/-}$ mice exposed to bright light exhibit a rapid increase in levels of atRAL in the retina and an acceleration of photoreceptor damage (5, 11, 12). Our research has indicated that light-induced photoreceptor degeneration and apoptosis in *Abca4*$^{-/-}$*Rdh8*$^{-/-}$ mice involves activation of c-Jun N-terminal kinase (JNK) signaling by atRAL (6). Ferroptosis is an iron-dependent and nonapoptotic form of cell death (13). Most recently, we provided evidence that ferroptotic cell death caused by atRAL drives photoreceptor atrophy in light-exposed *Abca4*$^{-/-}$*Rdh8*$^{-/-}$ mice (7).

The gasdermins (GSDMs), including GSDMA, GSDMB, GSDMC, GSDMD, and GSDME (also known as DFNA5), are a family of pore-forming effector proteins that serve as direct executioners of pyroptosis, a type of programmed cell death (PCD) characterized by cell swelling, pore formation on the plasma membrane, plasma membrane rupture, and release of cytosolic contents, such as high-mobility group box 1 (HMGB1) (14–20). GSDM proteins contain an amino-terminal pore-forming domain (GSDM-N) responsible for inducing pyroptosis through perforating the plasma membrane and a carboxyterminal autoinhibitory domain (GSDM-C) that functions to repress GSDM-N activity (16, 21, 22). Previous studies have shown that cleavage of GSDMD by

* For correspondence: Yalin Wu, yalinw@xmu.edu.cn.

inflammatory caspase-1/4/5/11 and cleavage of GSDME by apoptotic caspase-3, respectively, give rise to GSDMD-N and N-terminal fragment of GSDME (GSDME-N), each of which subsequently executes pyroptosis (15, 23–27). However, to the best of our knowledge, the relationship of pyroptosis to dry AMD and STGD1 remains elusive. In this publication, we report that GSDME but not GSDMD plays a crucial role in photoreceptor degeneration in retinopathies that feature disrupted clearance of atRAL.

Results

Photoinduced photoreceptor degeneration in $Abca4^{-/-}Rdh8^{-/-}$ *mice involves GSDME activation capable of eliciting pyroptosis and apoptosis, but it is independent of necroptosis*

About 48-h dark-adapted C57BL/6J WT, $Abca4^{-/-}Rdh8^{-/-}$, $Gsdme^{-/-}$, and $Abca4^{-/-}Rdh8^{-/-}Gsdme^{-/-}$ mice aged 4 weeks were irradiated as we previously described (6, 7). Eyeballs were collected at day 5 upon light exposure. The visual pigment rhodopsin constitutes approximately 90% and 75% of total proteins in disc and plasma membranes of photoreceptor OSs, respectively (1). Confocal immunofluorescence staining using an antirhodopsin antibody revealed a significant reduction in rhodopsin protein levels and OS thickness in neural retina of $Abca4^{-/-}Rdh8^{-/-}$ mice after light exposure (Fig. 1*A*). Immunofluorescence analysis of neural retina from light-exposed $Abca4^{-/-}Rdh8^{-/-}$ mice by confocal microscopy demonstrated the induction of GSDME-N, a direct executioner of pyroptosis, in photoreceptor outer nuclear layer (ONL) (Fig. 1*B*). Phosphorylated mixed lineage kinase domain-like protein (p-MLKL) is a representative activation marker of necroptosis (28, 29). It was interesting to observe that protein levels of p-MLKL were unchanged in neural retina of light-exposed $Abca4^{-/-}Rdh8^{-/-}$ mice (Fig. 1*C*). Lately, we present evidence that protein levels of cleaved caspase-3 in association with photoreceptor apoptosis caused by atRAL are notably upregulated in neural retina of $Abca4^{-/-}Rdh8^{-/-}$ mice following exposure to light (6). However, caspase-3 activation was significantly inhibited in neural retina of $Abca4^{-/-}Rdh8^{-/-}Gsdme^{-/-}$ mice upon light exposure (Fig. 1*D*). Consistent with our most recently published articles (6, 7), histological evaluations with H&E staining uncovered that neural retina of $Abca4^{-/-}Rdh8^{-/-}$ mice exposed to light was severely disrupted compared with that of C57BL/6J WT mice, particularly OS, inner segment (IS), and ONL of photoreceptors (Fig. 1*E*). It is worth mentioning that neural retina of $Gsdme^{-/-}$ mice and light-exposed C57BL/6J WT and $Gsdme^{-/-}$ mice was unaffected in comparison with that of C57BL/6J WT mice (Fig. 1, *E* and *F*). More importantly, knocking out *Gsdme* gene in $Abca4^{-/-}Rdh8^{-/-}$ mice effectively ameliorated photoreceptor atrophy and prevented the reduction in the thickness of whole neural retina, ONL and IS + OS in $Abca4^{-/-}Rdh8^{-/-}$ mice in response to light exposure (Fig. 1, *E* and *F*). Moreover, genotypes of C57BL/6J WT, $Abca4^{-/-}Rdh8^{-/-}$, $Gsdme^{-/-}$, and $Abca4^{-/-}Rdh8^{-/-}Gsdme^{-/-}$ mice that did not contain the *rd8* mutation in *Crb1* gene were identified by PCR, genome sequencing, and Western blotting (Fig. 1*G*). These findings imply that photoreceptor damage in mice characterized by an interruption in atRAL clearance is closely related to GSDME-dependent pyroptosis and apoptosis, but it does not depend on necroptosis.

atRAL enters 661W photoreceptor cells, and its cytotoxicity depends on the aldehyde group

Cone photoreceptor cell line 661W, derived from a mouse retinal tumor (30), was purchased from Shanghai Zishi Biotechnology and further characterized by mRNA expression of OPN1SW, a specific marker of cone photoreceptors (Fig. S1). Uptake of atRAL (λmax = 380 nm) and atROL (λmax = 325 nm) by 661W photoreceptor cells was confirmed by analysis of intracellular granules by HPLC (Fig. 2, *A* and *B*). It is well known that atROL forms by reduction of the aldehyde group in atRAL to an alcohol group (31). The results of MTS assay demonstrated that exposure of 661W photoreceptor cells to 5 μM of atRAL for 6 h resulted in a clear decline in cell viability (Fig. 2*C*), but atROL did not affect the health of 661W photoreceptor cells at concentrations ranging from 5 to 20 μM (Fig. 2*C*). Moreover, a peak attributable to atROL was also observed in the HPLC chromatogram obtained from extracts of 661W photoreceptor cells incubated for 6 h with 5 μM of atRAL (Fig. 2*A*), indicating that some of atRAL are converted into atROL, probably by RDH8. To further corroborate the effect of RDH8 on atRAL entering cells, 661W photoreceptor cells with RDH8 overexpression were treated with 5 μM of atRAL for 6 h (Fig. 2, *D*–*H*). HPLC analysis of extracts from atRAL-loaded RDH8-overexpressing 661W photoreceptor cells showed that peak height of atROL (monitored at 325 nm) was significantly elevated, but atRAL peak height (monitored at 380 nm) was remarkably decreased (Fig. 2, *E* and *F*). Consistently, quantification by integrating peak areas revealed an approximately 4.6-fold increase in atROL levels and a reduction of atRAL levels by approximately 73% in RDH8-overexpressing 661W photoreceptor cells in response to atRAL (Fig. 2*G*). As expected, overexpression of RDH8 protein dramatically promoted the survival of 661W photoreceptor cells exposed to atRAL (Fig. 2*H*). These lines of evidence suggest that atRAL is capable of being internalized by 661W photoreceptor cells, and its aldehyde group is responsible for cellular toxicity.

Activation of GSDME but not GSDMD induces pyroptosis and requires caspase-3 activation in atRAL-loaded 661W photoreceptor cells

661W photoreceptor cells were utilized as an *in vitro* model for ascertaining the role of GSDME in photoreceptor degeneration in mice with defects in atRAL clearance. Moreover, 5 μM of atRAL was used to treat 661W photoreceptor cells for 6 h in subsequent experiments, which could be explained by our previous reports (6, 7). On examination by microscopy, dying atRAL-loaded 661W photoreceptor cells displayed morphological characteristics of pyroptosis, such as cell swelling with large bubbles emanating from the plasma

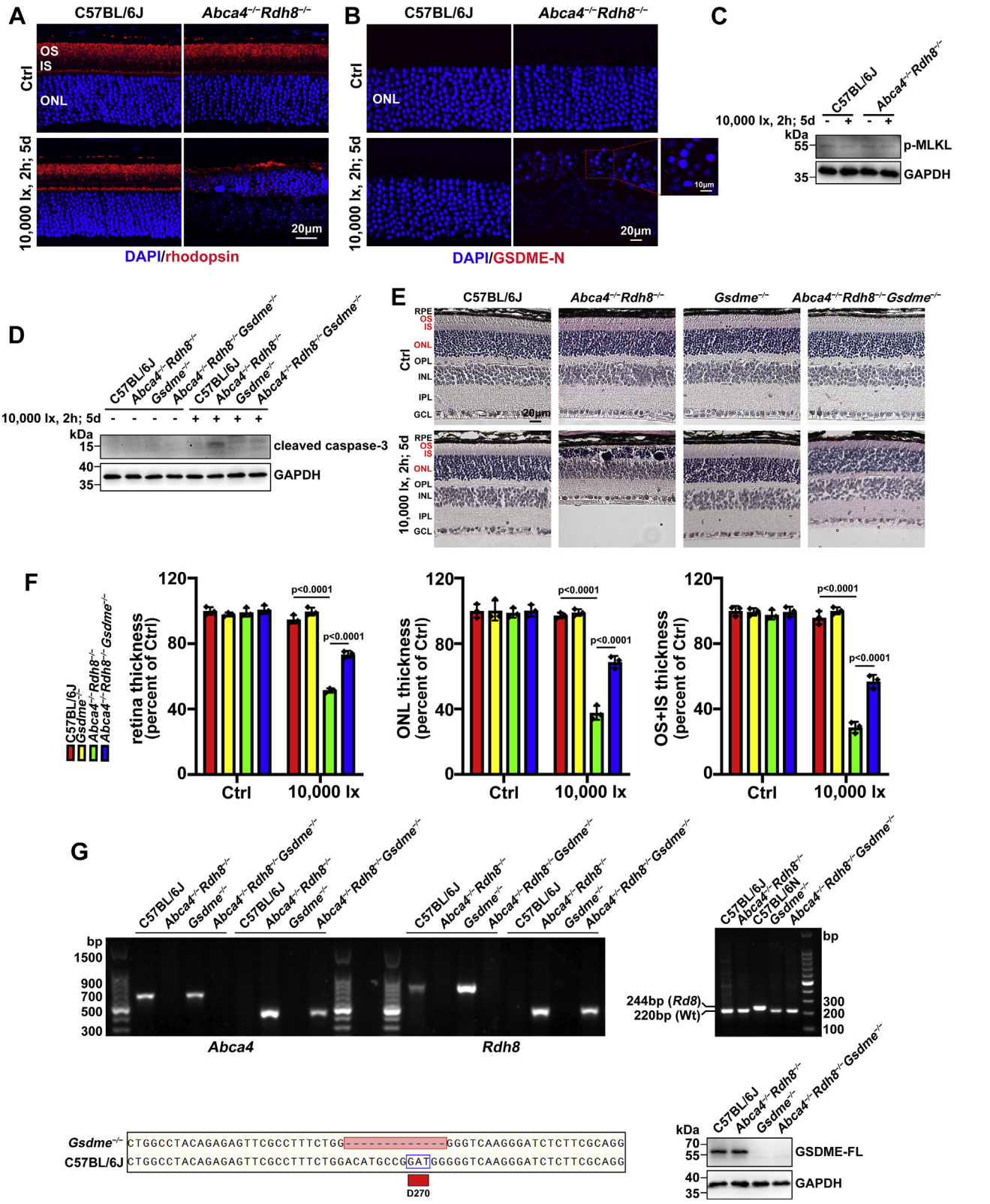

Figure 1. Light-induced photoreceptor degeneration in *Abca4*$^{-/-}$*Rdh8*$^{-/-}$ mice involves GSDME activation leading to pyroptosis and apoptosis, but it is unrelated to necroptosis. Four-week-old C57BL/6J WT, *Abca4*$^{-/-}$*Rdh8*$^{-/-}$, *Gsdme*$^{-/-}$, and *Abca4*$^{-/-}$*Rdh8*$^{-/-}$*Gsdme*$^{-/-}$ mice were placed in a dark room for 2 days. After pupils of dark-adapted mice were dilated with 1% tropicamide, they were exposed to 10,000 lx light-emitting diode light for 2 h and then kept in the dark for 5 days. Control C57BL/6J WT, *Abca4*$^{-/-}$*Rdh8*$^{-/-}$, *Gsdme*$^{-/-}$, and *Abca4*$^{-/-}$*Rdh8*$^{-/-}$*Gsdme*$^{-/-}$ mice were maintained normally in the dark for 7 days in the absence of light exposure. *A*, the morphology of photoreceptor OSs in mouse retina was evaluated by immunofluorescence staining for rhodopsin (*red*). Nuclei were stained with DAPI (*blue*). The scale bars represent 20 μm. *B*, protein levels of GSDME-N in photoreceptor ONL were determined by immunofluorescence staining of mouse retina with an anti-GSDME-N antibody (*red*). Nuclei were stained *blue* with DAPI. The scale bars represent 20 and 10 μm. *C* and *D*, immunoblotting was utilized to assess protein levels of p-MLKL and cleaved caspase-3 in extracts from neural retina. *E*, the histology of

membrane (Fig. 3*A*). Determination of plasma membrane integrity by lactate dehydrogenase (LDH) release assay disclosed that atRAL remarkably evoked the release of LDH from 661W photoreceptor cells (Fig. 3*B*). Western blot analysis also showed that 661W photoreceptor cells upon exposure to atRAL significantly released HMGB1 (Fig. 3, *C* and *D*), further confirming the ability of atRAL to trigger plasma membrane rupture and leakage. GSDMD and GSDME have been identified as direct pyroptotic executioners (15, 27). Immunoblot analysis demonstrated that GSDME-N was clearly present in cell lysates of 661W photoreceptor cells in response to atRAL, but no cleavage of GSDMD was observed (Fig. 3, *E* and *F*), indicating the involvement of GSDME rather than GSDMD in atRAL-induced photoreceptor pyroptosis. Given that pyroptosis and necroptosis are two forms of PCD with common features of cell swelling, plasma membrane disruption, and lysis (17, 32), necrostatin-1 (Nec-1), a potent inhibitor of necroptosis, was employed to distinguish pyroptosis from necroptosis in atRAL-loaded 661W photoreceptor cells. The results showed that treatment with Nec-1 at a concentration of 50 μM did not prevent LDH release from 661W photoreceptor cells following 6 h of exposure to 5 μM of atRAL, and likewise, it failed to enhance cell viability (Fig. 3, *G* and *H*), suggesting that necroptosis is not involved in photoreceptor cell death caused by atRAL. Caspase-3 activation has been reported to be capable of cleaving GSDME (27). Consistent with a previous study by our laboratory (6), protein levels of cleaved caspase-3 were dramatically elevated in cell lysates of 661W photoreceptor cells upon atRAL exposure (Fig. 3, *I* and *J*). To further verify that active caspase-3 cleaves and activates GSDME to stimulate pyroptosis caused by atRAL, we used caspase-3-targeted siRNA to efficiently knock down caspase-3 expression in 661W photoreceptor cells, as evidenced by quantitative real-time PCR (qRT–PCR) and Western blotting (Fig. 3, *K* and *L*). Visualization of cell morphology by microscopy revealed that silence of caspase-3 significantly attenuated pyroptotic cell death in atRAL-loaded 661W photoreceptor cells (Fig. 3*M*). In addition, caspase-3 knockdown visibly repressed LDH release from 661W photoreceptor cells in response to atRAL (Fig. 3*N*), and it clearly increased cell viability (Fig. 3*O*). Western blot analysis also indicated that silencing caspase-3 markedly restricted the generation of cleaved caspase-3 and GSDME-N in cell lysates and release of HMGB1 in culture supernatants from 661W photoreceptor cells after 6 h of exposure to 5 μM of atRAL (Fig. 3, *P* and *Q*). Taken together, we provide strong evidence that activation of GSDME but not GSDMD promotes atRAL-induced photoreceptor pyroptosis, and it demands activation of caspase-3.

Knockout of Gsdme *gene protects 661W photoreceptor cells exposed to atRAL* via *blocking caspase-3–GSDME activation*

To further corroborate the role of GSDME in atRAL-induced cell death, especially pyroptosis, *Gsdme* gene was knocked out in 661W photoreceptor cells using the CRISPR–Cas9 technology. A deficient expression of GSDME-full-length (FL) protein in cell lysates of 661W photoreceptor cells lacking *Gsdme* gene (*Gsdme*$^{-/-}$ 661W photoreceptor cells) was documented by Western blotting (Fig. 4*A*). Genetic deletion of *Gsdme* gene significantly inhibited the release of LDH from 661W photoreceptor cells following 6 h of exposure to 5 μM of atRAL, and it clearly promoted cell survival (Fig. 4, *B* and *C*). Moreover, confocal microscopic examination showed that knockout of *Gsdme* gene reversed damage to the morphology of 661W photoreceptor cells upon atRAL exposure (Fig. 4*D*). SYTOX Orange dead cell stain is a high-affinity nucleic acid dye that readily penetrates cells with ruptured plasma membrane and yet is unable to cross healthy cell membrane. The formation of pores in the plasma membrane of cells undergoing pyroptosis allows SYTOX Orange dead cell stain that exhibits red fluorescence with excitation at 530 nm and emission at 570 nm to enter pyroptotic cells and stain nuclei. SYTOX Orange staining coupled with fluorescence microscopy showed that pyroptosis was visibly weakened in atRAL-loaded *Gsdme*$^{-/-}$ *versus* WT 661W photoreceptor cells (Fig. 4*E*). As revealed by Western blotting, GSDME-N was absent in cell lysates of *Gsdme*$^{-/-}$ 661W photoreceptor cells following atRAL exposure (Fig. 4*F*). Interestingly, protein levels of cleaved caspase-3 were found to be significantly decreased in atRAL-exposed *Gsdme*$^{-/-}$ compared with WT 661W photoreceptor cells (Fig. 4, *F* and *G*), suggesting that GSDME also functions upstream of caspase-3, and its activation may facilitate apoptosis through aggravating caspase-3 activation (33, 34). Poly-ADP-ribose polymerase (PARP) is a nuclear enzyme that serves as a death substrate for caspase-3 in apoptosis (35). Immunoblot analysis showed that knocking out GSDME significantly attenuated protein levels of cleaved PARP in cell lysates of atRAL-loaded 661W photoreceptor cells (Fig. 4, *F* and *G*), thereby further confirming that activation of GSDME by atRAL indeed implicates caspase-dependent apoptotic cell death. As expected, elimination of

mouse retina was examined by H&E staining. The scale bars represent 20 μm. *F*, thickness of whole retina ($F_{0.05}$ (3,16) = 153.1; $p < 0.0001$), ONL ($F_{0.05}$ (3,16) = 83.28; $p < 0.0001$), or IS + OS ($F_{0.05}$ (3,16) = 161.4; $p < 0.0001$) was quantified by Leica Application Suite X microscope software and expressed as a percentage of that measured in control C57BL/6J WT mice without exposure to light. Statistical analyses were performed by using two-way ANOVA with Tukey's post-test. *G*, genotyping of *Abca4*$^{-/-}$*Rdh8*$^{-/-}$, *Gsdme*$^{-/-}$, and *Abca4*$^{-/-}$*Rdh8*$^{-/-}$*Gsdme*$^{-/-}$ mice with a C57BL/6J genetic background was performed by PCR amplification of tail DNAs with specific primers. In a previous report from our laboratory, we have shown a detailed textual description for PCR analysis of *Abca4* and *Rdh8* gene deletions and the absence of *rd8* mutation in the *Crb1* gene in mice (6). C57BL/6N mice carrying *Rd8* mutation of the *Crb1* gene served as a positive control. Diagrammatic representation of a part of gene sequence in the seventh exon of *Gsdme* that locates in chromosome 6 from C57BL/6J WT and *Gsdme*$^{-/-}$ mice. Compared with C57BL/6J WT mice, the sequence of the gene encoding GSDME in *Gsdme*$^{-/-}$ mice lacks 13 bp in which D270, the caspase-3 recognition motif, is included. Western blotting was used to analyze GSDME-FL expression in neural retina of C57BL/6J WT, *Abca4*$^{-/-}$*Rdh8*$^{-/-}$, *Gsdme*$^{-/-}$, and *Abca4*$^{-/-}$*Rdh8*$^{-/-}$*Gsdme*$^{-/-}$ mice. GAPDH in *C*, *D*, and *G* was used as an internal control. Molecular mass markers (kilodalton) in *C*, *D*, and *G* were indicated to the *left* of immunoblots. Results in *A*–*G* are from at least three mice per group. DAPI, 4′,6-diamidino-2-phenylindole; GCL, ganglion cell layer; GSDME, gasdermin E; GSDME-N, N-terminal fragment of GSDME; INL, inner nuclear layer; IPL, inner plexiform layer; IS, inner segment; p-MLKL, phosphorylated mixed lineage kinase domain-like protein; RPE, retinal pigment epithelium; ONL, outer nuclear layer; OPL, outer plexiform layer; OS, outer segment.

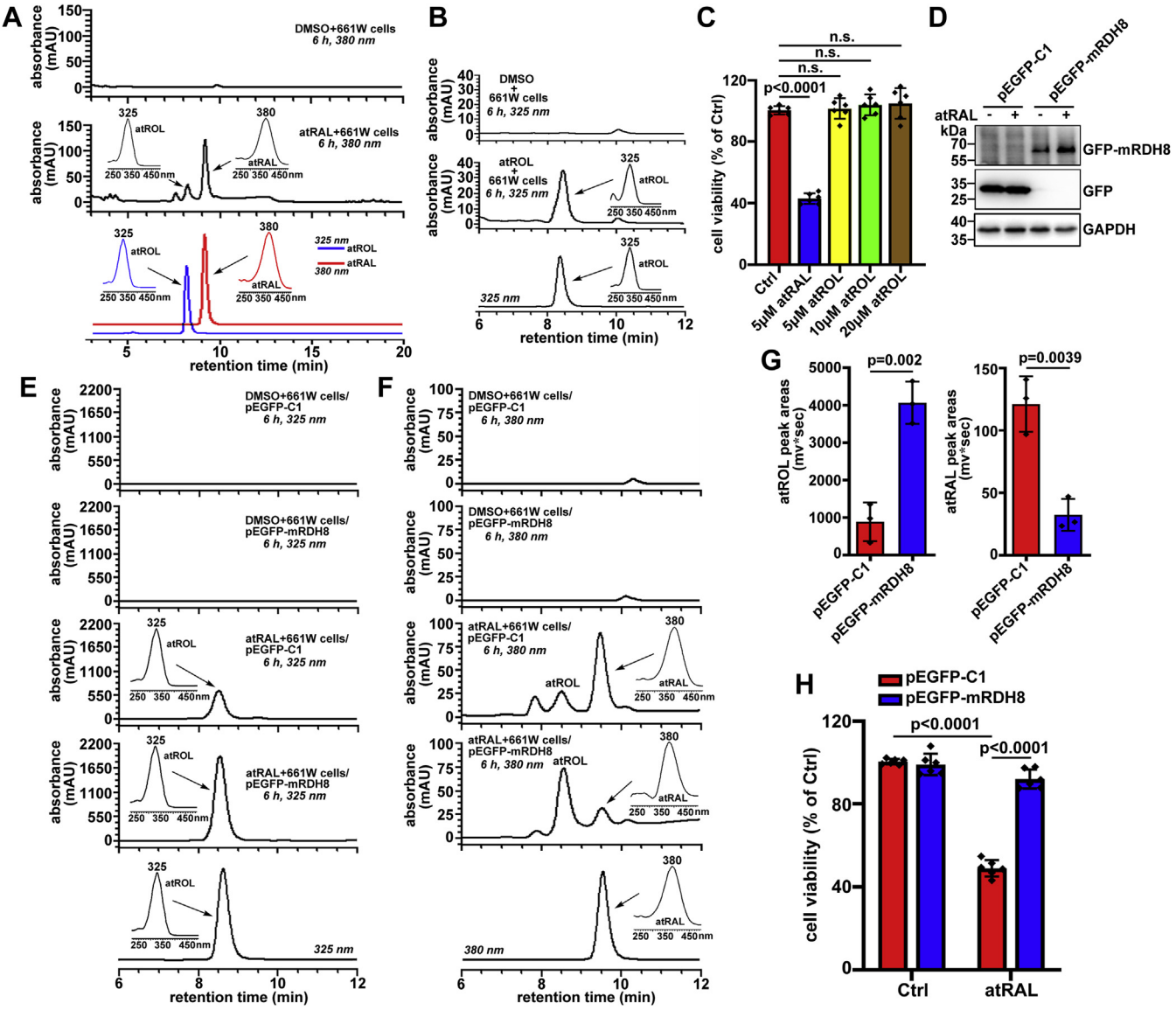

Figure 2. atRAL is internalized, and its aldehyde group mediates cytotoxicity to 661W photoreceptor cells. *A*, internalization of atRAL. Typical HPLC chromatograms (dC18 column, monitoring at 380 nm) were generated with extracts of 661W photoreceptor cells treated with 5 μM of atRAL or DMSO (vehicle) alone for 6 h. Commercially available atRAL (monitored at 380 nm) and atROL (monitored at 325 nm) served as controls. *Insets* in *middle* and *lower panels*, UV–visible absorbance spectra of atROL and atRAL. *B*, internalization of atROL. Representative HPLC chromatograms (dC18 column, monitoring at 325 nm) were obtained from extracts of 661W photoreceptor cells exposed for 6 h to 5 μM of atROL and DMSO alone, respectively, as well as a moderate amount of atROL standard. *Right insets* in *middle* and *lower panels*, UV–visible absorbance spectra of atROL. *C*, cytotoxicity was probed by MTS assay. 661W photoreceptor cells were incubated for 6 h with atRAL (5 μM), atROL (5, 10, and 20 μM), or DMSO alone. $F_{0.05}$ (4,25) = 102.3, $p < 0.0001$. *D*, intracellular overexpression of RDH8. Western blotting was used to analyze protein levels of GFP-mRDH8 and GFP in cell lysates of 661W photoreceptor cells that were transfected with pEGFP-mRDH8 or vector pEGFP-C1 for 24 h and then treated for 6 h with 5 μM of atRAL and DMSO alone, respectively. *E* and *F*, typical HPLC profiles monitored at 325 (*E*) and 380 (*F*) nm were generated from extracts of RDH8-overexpressing 661W photoreceptor cells incubated with 5 μM of atRAL or DMSO alone for 6 h. Control cells were transfected with vector pEGFP-C1 and then treated for 6 h with 5 μM of atRAL or DMSO alone. *Insets* in the last three panels of *A* and *B*, UV–visible absorbance spectra of atROL and atRAL. *G*, quantification of atROL (monitored at 325 nm) and atRAL (monitored at 380 nm) in RDH8-overexpressing and control vector–transfected 661W photoreceptor cells that were treated with 5 μM of atRAL for 6 h, respectively. Empower version 3 software was applied for measuring the integrated peak areas of atROL and atRAL. *mv*sec*, millivolts*seconds. *H*, cell viability, 6 h after exposure of 661W photoreceptor cells overexpressing RDH8 or transfected with vector pEGFP-C1 to 5 μM of atRAL, was detected by MTS assay. Cells treated with DMSO alone served as controls. $F_{0.05}$ (1,20) = 181.7, $p < 0.0001$. One-way ANOVA with Tukey's post-test in *C*, Student's *t* test in *G*, and two-way ANOVA with Tukey's post-test in *H* were performed for statistical analyses. atRAL, all-*trans*-retinal; atROL, all-*trans*-retinol; DMSO, dimethyl sulfoxide; ns, not significant; RDH8, all-*trans*-retinol dehydrogenase 8.

Gsdme gene dramatically reduced HMGB1 release in culture supernatants from 661W photoreceptor cells in response to atRAL (Fig. 4, *H* and *I*). These lines of evidence reflect that GSDME activation triggers photoreceptor loss caused by atRAL through inducing both pyroptosis and apoptosis.

Complete elimination of Gsdme *gene mitigates mitochondrial disruption in 661 photoreceptor cells in response to atRAL through inactivating GSDME*

WT or *Gsdme*$^{-/-}$ 661W photoreceptor cells treated for 6 h with 5 μM of atRAL were fractionated into mitochondrial and

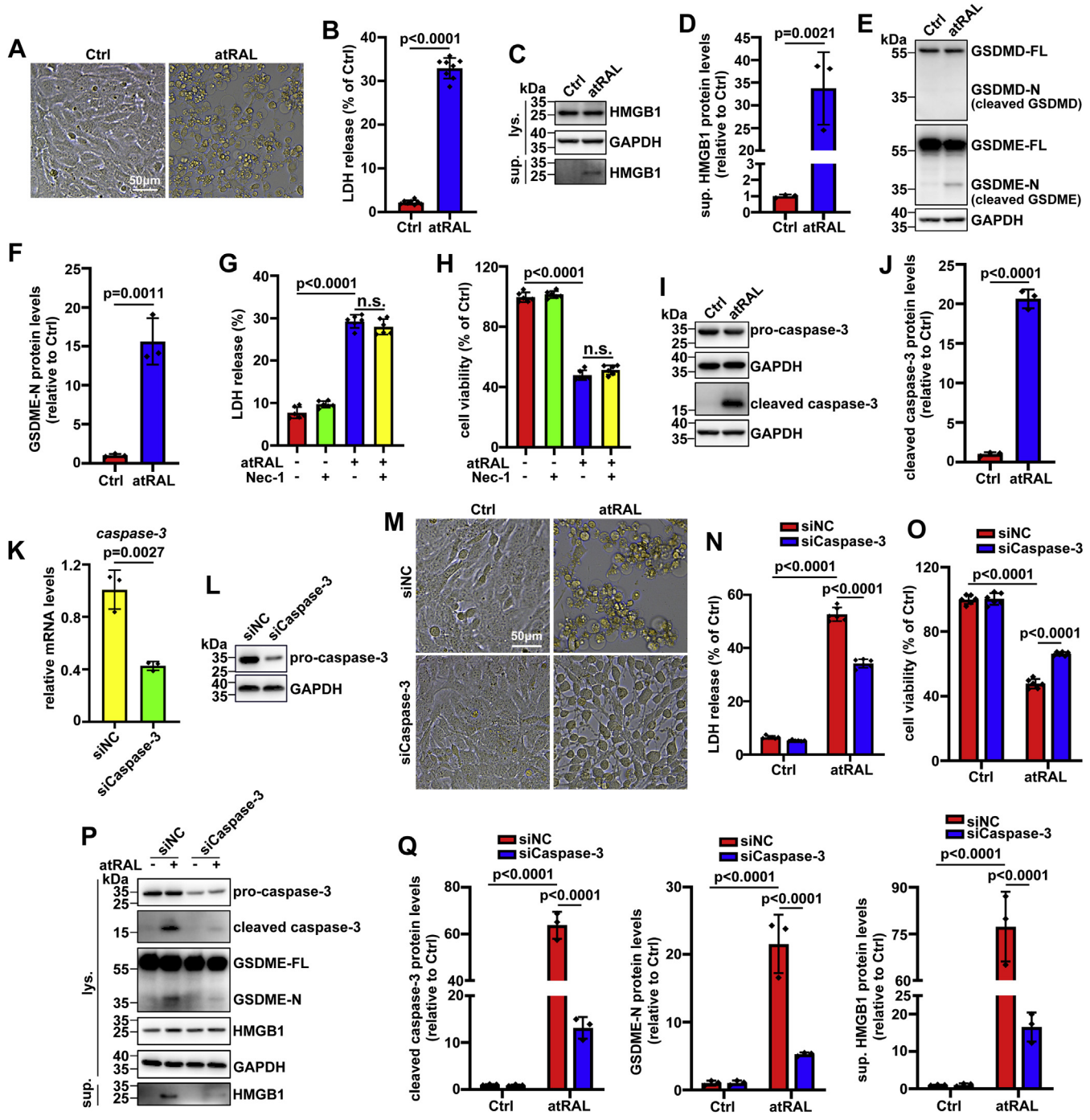

Figure 3. Activation of GSDME by caspase-3 promotes atRAL-induced pyroptosis of 661W photoreceptor cells. *A*, representative microscopic images of 661W photoreceptor cells following 6 h of exposure to 5 μM of atRAL were taken using a Leica DM2500 microscope. Control cells were incubated with DMSO alone. The scale bars represent 50 μm. *B*, rupture of the plasma membrane was analyzed using LDH release assay. 661W photoreceptor cells were incubated with 5 μM of atRAL or DMSO alone for 6 h. *C*, immunoblotting was used to examine protein levels of HMGB1 in cell lysates or culture supernatants from 661W photoreceptor cells incubated with 5 μM of atRAL or DMSO alone for 6 h. The positions of molecular mass markers (kilodalton) are shown on the *left* of the blots. *D*, protein levels of HMGB1 in culture supernatants (sup. HMGB1) were normalized to those of GAPDH and expressed as fold changes relative to DMSO-treated controls. *E*, cell lysates of 661W photoreceptor cells following 6 h of exposure to 5 μM of atRAL or DMSO alone were analyzed by Western blotting. The blots were probed with antibodies against GSDMD and GSDME, respectively. *F*, levels of GSDME-N protein were normalized to those of GAPDH and presented as fold changes relative to DMSO-treated controls. *G*, rupture of the plasma membrane was evaluated by LDH release assay. 661W photoreceptor cells were pretreated with 50 μM of Nec-1 for 1 h and then incubated with 5 μM of atRAL for 6 h. Control cells were exposed to atRAL, Nec-1, or DMSO alone. $F_{0.05}$ (3,20) = 393.8, $p < 0.0001$. *H*, cytotoxicity was examined by MTS assay. 661W photoreceptor cells were treated with 5 μM of atRAL for 6 h in the presence of 50 μM of Nec-1. Note that cells were pretreated with Nec-1 for 1 h. $F_{0.05}$ (3,20) = 577.7, $p < 0.0001$. *I*, Western blot analysis of procaspase-3 and cleaved caspase-3 in cell lysates of 661W photoreceptor cells incubated with 5 μM of atRAL or DMSO alone for 6 h. *J*, protein levels of cleaved caspase-3 were normalized to those of GAPDH and presented as fold changes relative to DMSO-treated controls. *K* and *L*, qRT–PCR and Western blotting were used to assess the knockdown efficiency of caspase-3 in 661W photoreceptor cells with siRNA specific for caspase-3. Cells transfected with caspase-3 siRNA (siCaspase-3) or negative control (NC) siRNA (siNC) were harvested at 24 h post-transfection. *M*, typical microscopic photographs of siNC-transfected or siCaspase-3-transfected 661W photoreceptor cells treated with 5 μM of atRAL or DMSO alone for 6 h. The scale bars represent 50 μm. *N*, rupture of the plasma membrane was examined using LDH release assay. 661W photoreceptor cells were transfected with siNC or

cytosolic fractions for immunoblot analysis of GSDME-N and cytochrome *c* (Cyt *c*), respectively. We found significant increases in protein levels of GSDME-N in the mitochondria and GSDME-N and Cyt *c* in the cytosol from atRAL-loaded WT 661W photoreceptor cells (Figs. S2 and 5, *A* and *B*). Conversely, a deficiency of GSDME-N in both the cytosol and mitochondria, reduced protein levels of cytosolic Cyt *c*, and increased protein levels of mitochondrial Cyt *c* were significantly observed in atRAL-loaded *Gsdme*$^{-/-}$ *versus* WT 661W photoreceptor cells (Fig. 5, *A* and *B*), implying that GSDME-N generated by atRAL in photoreceptor cells partially localizes to mitochondria and perforates in mitochondrial membranes, thus eliciting Cyt *c* release into the cytosol (33, 34). On examination by transmission electron microscopy (TEM), disruption in mitochondrial membranes was severely induced by atRAL in WT 661W photoreceptor cells, but it was visibly alleviated in atRAL-loaded *Gsdme*$^{-/-}$ 661W photoreceptor cells (Fig. 5*C*). Lately, we report that atRAL promotes photoreceptor apoptosis through caspase-9 and caspase-3 cascade activation (6). Previous studies have indicated that Cyt *c* released into the cytosol helps to form apoptosomes containing Cyt *c*, Apaf-1, and caspase-9, leading to caspase-9 activation that cleaves and activates caspase-3 to provoke apoptosis (14). Taken together, these data suggest that activation of GSDME stimulates both pyroptosis and apoptosis in photoreceptor cells in response to atRAL *via* a mitochondria-mediated caspase-dependent signaling pathway.

Genetic deletion of Jnk1 *and* Jnk2 *genes attenuates plasma membrane rupture in atRAL-loaded 661W photoreceptor cells through repressing activation of GSDME by caspase-3*

We have recently described that activation of JNK signaling by atRAL evokes photoreceptor apoptosis (6), but we wonder whether it also participates in pyroptotic cell death in photoreceptor cells. Interestingly, there was a remarkable reduction in release of LDH and HMGB1 from atRAL-loaded *Jnk1*$^{-/-}$*Jnk2*$^{-/-}$ *versus* WT 661W photoreceptor cells (Fig. 6, *A*–*C*), indicating that complete inhibition of JNK activation caused by atRAL dramatically prevents disruption of the plasma membrane. Besides, exposure of *Jnk1*$^{-/-}$*Jnk2*$^{-/-}$ 661W photoreceptor cells to 5 μM of atRAL for 6 h resulted in significantly decreased protein levels of cleaved caspase-3 and GSDME-N in cell lysates of 661W photoreceptor cells (Fig. 6, *D* and *E*). As expected, immunoblot analysis revealed an absence of p-JNK and JNK in cell lysates of *Jnk1*$^{-/-}$*Jnk2*$^{-/-}$ 661W photoreceptor cells regardless of atRAL exposure (Fig. 6*D*). Overall, these findings suggest that JNK is upstream of GSDME, and its activation triggers atRAL-induced photoreceptor pyroptosis through eliciting activation of GSDME by caspase-3.

Inhibition of reactive oxygen species production mitigates pyroptosis in atRAL-loaded 661W photoreceptor cells by reducing caspase-3-dependent activation of GSDME

We have lately shown that reactive oxygen species (ROS) production is one of the initiators for JNK activation associated with photoreceptor apoptosis induced by atRAL (6). Moreover, treatment with ROS scavenger *N*-acetyl-L-cysteine (NAC) at a concentration of 2 mM has been reported to effectively attenuate ROS production and JNK activation in 661W photoreceptor cells following 6 h of exposure to 5 μM of atRAL, and it moderately enhances cell viability (6). In the current study, it was found that 2 mM of NAC prevented the release of LDH and HMGB1 from 661W photoreceptor cells in response to atRAL (Fig. 7, *A*–*C*). More importantly, Western blot analysis indicated that protein levels of cleaved caspase-3 and GSDME-N were obviously downregulated by 2 mM of NAC in cell lysates of atRAL-loaded 661W photoreceptor cells (Fig. 7, *D* and *E*). These results imply that ROS production initiated by atRAL stimulates caspase-3–GSDME-dependent photoreceptor pyroptosis at least partially through activating JNK signaling.

Discussion

Over the past decades, some forms of PCD in mammals have been recognized, mainly including apoptosis, necroptosis, pyroptosis, and ferroptosis (14). Two types of PCD, apoptosis and ferroptosis, have been identified in the development of photoreceptor degeneration in mice featuring defective atRAL clearance in association with dry AMD and STGD1 for which there are presently no approved cures (6, 7). In this article, we documented GSDME-dependent photoreceptor pyroptosis and apoptosis upon activation of caspase-3 by atRAL. On the contrary, unchanged phosphorylation of MLKL, a direct executioner of plasma membrane rupture in necroptosis (28, 29), in neural retina of *Abca4*$^{-/-}$*Rdh8*$^{-/-}$ mice following light exposure (Fig. 1*C*), together with the inability of necroptosis inhibitor Nec-1 to rescue 661W photoreceptor cells in response to atRAL (Fig. 3, *G* and *H*), indicated that necroptosis was not implicated in photoreceptor degeneration in retinopathies mediated by disrupted clearance of atRAL. No expression of receptor interacting protein kinase 3 (RIP3), the obligate upstream of MLKL in necroptosis (36), was observed in neural retina of C57BL/6J WT mice as well as neural retina and RPE of *Rip3*$^{-/-}$ mice (Fig. S3), which further suggests that

siCaspase-3 for 24 h and then incubated with 5 μM of atRAL and DMSO alone for 6 h, respectively. $F_{0.05}$ (1,20) = 187.5, $p < 0.0001$. *O*, cell viability was examined by MTS assay. 661W photoreceptor cells transfected with siNC or siCaspase-3 for 24 h were exposed for 6 h to 5 μM of atRAL and DMSO alone, respectively. $F_{0.05}$ (1,20) = 66.25, $p < 0.0001$. *P*, Western blotting was used to determine protein levels of procaspase-3, cleaved caspase-3, GSDME-FL, GSDME-N, and HMGB1 in cell lysates and HMGB1 in culture supernatants from siNC-transfected or siCaspase-3-transfected 661W photoreceptor cells treated for 6 h with 5 μM of atRAL and DMSO alone, respectively. *Q*, protein levels of cleaved caspase-3 ($F_{0.05}$ (1,8) = 197.6, $p < 0.0001$), GSDME-N ($F_{0.05}$ (1,8) = 42.41, $p = 0.0002$), and sup. HMGB1 ($F_{0.05}$ (1,8) = 78.52, $p < 0.0001$) were normalized to those of GAPDH and shown as fold changes relative to DMSO-treated controls. Student's *t* test in *B*, *D*, *F*, *J*, and *K*, one-way ANOVA with Tukey's post-test in *G* and *H* and two-way ANOVA with Tukey's post-test in *N*, *O*, and *Q* were performed for statistical analyses. atRAL, all-*trans*-retinal; DMSO, dimethyl sulfoxide; GSDMD, gasdermin D; GSDME, gasdermin E; GSDME-FL, full-length GSDME; GSDME-N, N-terminal fragment of GSDME; HMGB1, high-mobility group box 1; LDH, lactate dehydrogenase; lys., lysate; Nec-1, necrostatin-1; ns, nonsignificant; qRT–PCR, quantitative RT–PCR; sup., supernatant.

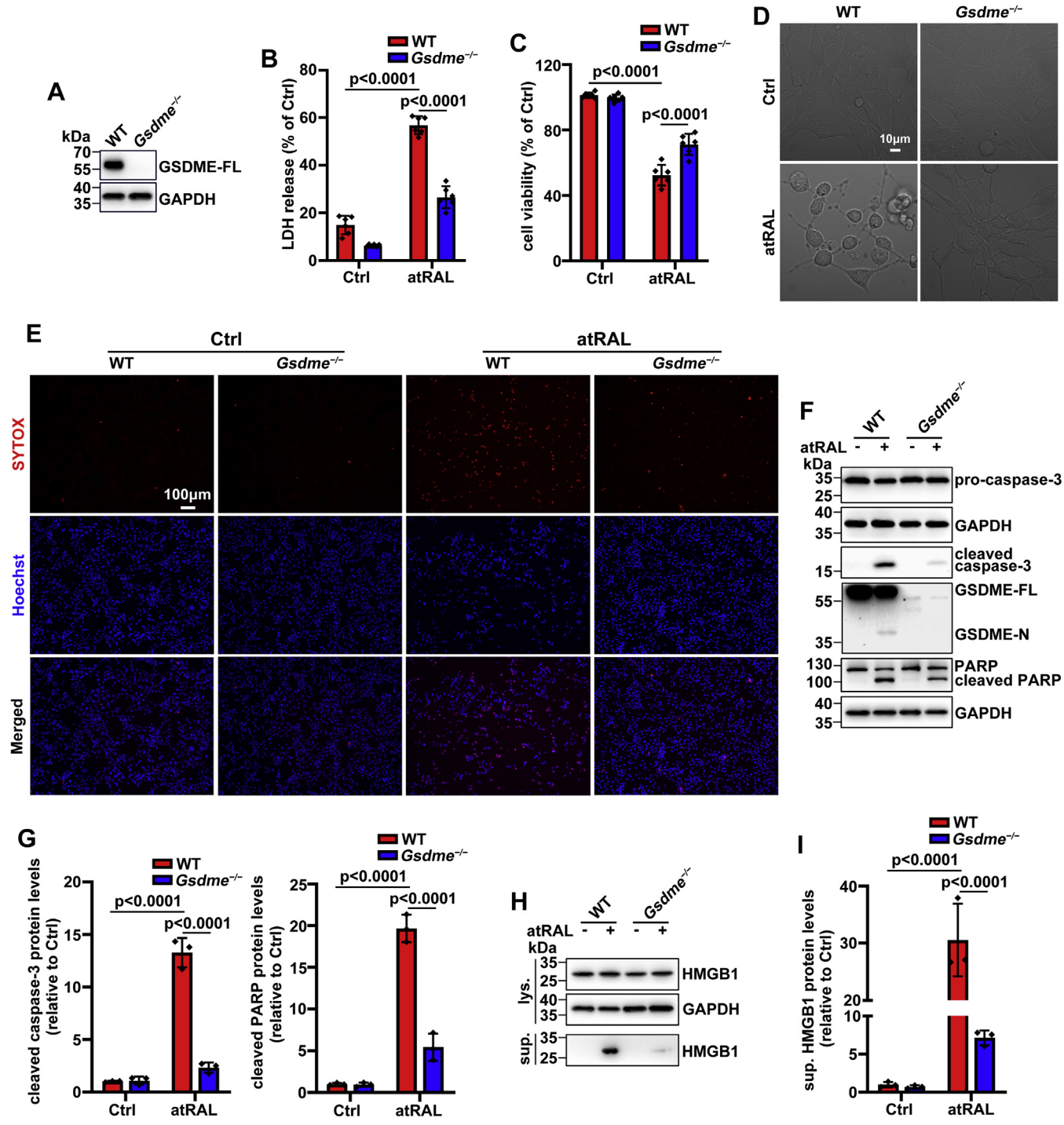

Figure 4. Knockout of *Gsdme* gene enhances the survival of 661W photoreceptor cells in response to atRAL. *A*, immunoblot analysis of GSDME-FL in cell lysates of WT or *Gsdme*$^{-/-}$ 661W photoreceptor cells. The positions of molecular mass markers (kilodalton) are indicated to the *left* of the blots. *B*, rupture of the plasma membrane was determined by LDH release assay. WT or *Gsdme*$^{-/-}$ 661W photoreceptor cells were incubated with 5 μM of atRAL and DMSO alone for 6 h, respectively. $F_{0.05}$ (1,20) = 55.33, $p < 0.0001$. *C*, cell viability, 6 h after exposure of WT or *Gsdme*$^{-/-}$ 661W photoreceptor cells to 5 μM of atRAL or DMSO alone, was measured by MTS assay. $F_{0.05}$ (1,20) = 28.45, $p < 0.0001$. *D*, confocal microscopy was used to evaluate the morphology of WT or *Gsdme*$^{-/-}$ 661W photoreceptor cells following 6 h of exposure to 5 μM of atRAL and DMSO alone, respectively. *E*, SYTOX-positive cells (*red*), 6 h after exposure of WT or *Gsdme*$^{-/-}$ 661W photoreceptor cells to 5 μM of atRAL or DMSO alone, were visualized by fluorescence microscopy. Nuclei were stained with Hoechst 33342 (*blue*). The scale bars represent 100 μm. *F* and *G*, Western blot analysis of procaspase-3, cleaved caspase-3, GSDME-FL, GSDME-N, PARP, and cleaved PARP in cell lysates of WT or *Gsdme*$^{-/-}$ 661W photoreceptor cells treated with 5 μM of atRAL and DMSO alone for 6 h, respectively. Protein levels of cleaved caspase-3 ($F_{0.05}$ (1,8) = 158.9, $p < 0.0001$) and cleaved PARP ($F_{0.05}$ (1,8) = 110.6, $p < 0.0001$) were normalized to those of GAPDH and expressed as fold changes relative to DMSO-treated WT controls. *H* and *I*, Western blotting was employed to analyze protein levels of HMGB1 in cell lysates or culture supernatants from WT or *Gsdme*$^{-/-}$ 661W photoreceptor cells following 6 h of exposure to 5 μM of atRAL and DMSO alone, respectively. Protein levels of sup. HMGB1 were normalized to those of GAPDH and presented as fold changes compared with DMSO-treated WT controls. $F_{0.05}$ (1,8) = 38.69, $p = 0.0003$. Statistical analyses in *B*, *C*, *G*, and *I* were assessed by two-way ANOVA with Tukey's post-test. GAPDH in *A*, *F*, and *H* served as an internal control. atRAL, all-*trans*-retinal; DMSO, dimethyl sulfoxide; GSDME-FL, full-length GSDME; GSDME-N, N-terminal fragment of GSDME; HMGB1, high-mobility group box 1; LDH, lactate dehydrogenase; PARP, poly-ADP-ribose polymerase; sup., supernatant.

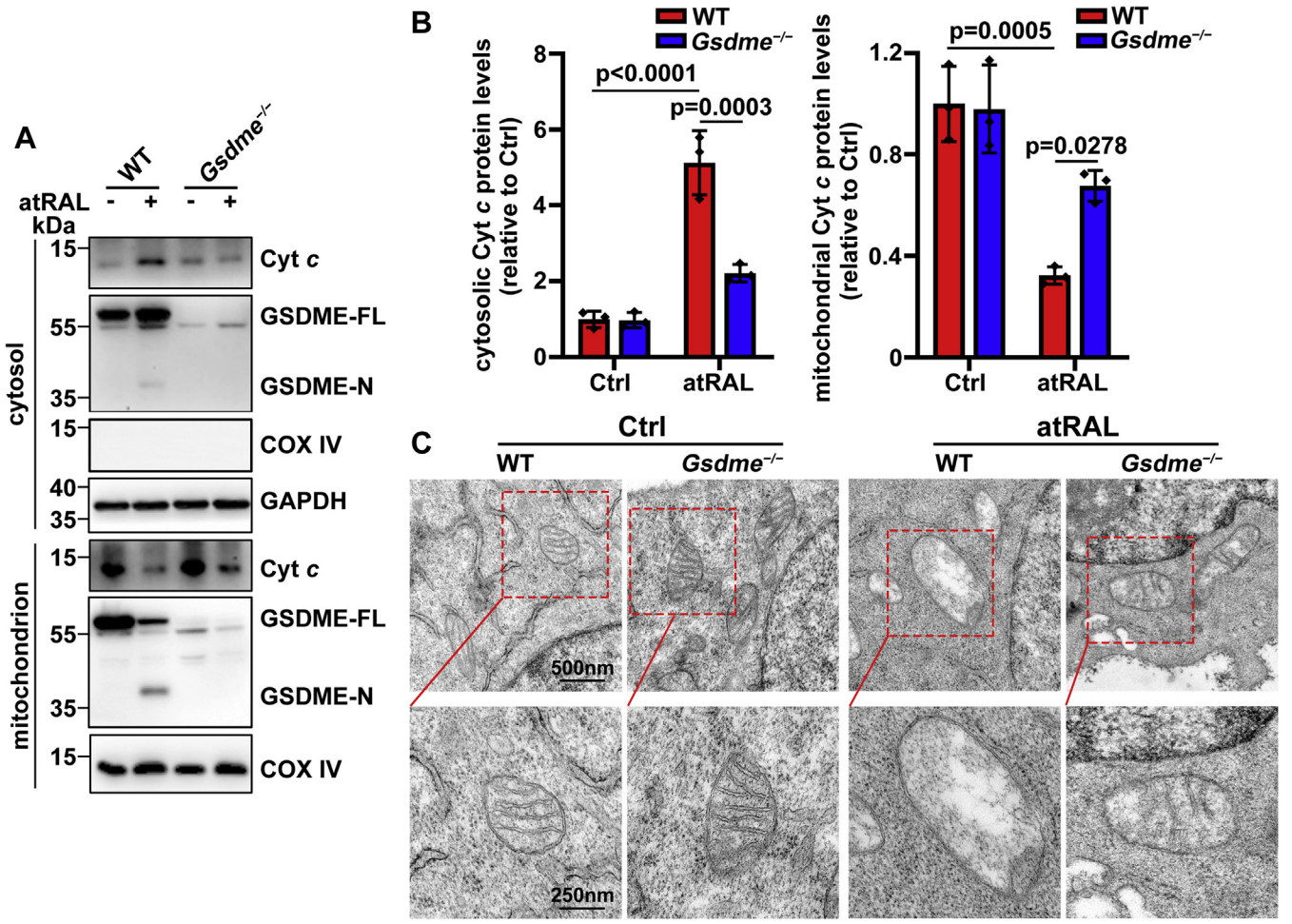

Figure 5. Deficiency of *Gsdme* gene protects mitochondria of 661W photoreceptor cells from damage caused by atRAL. *A*, Western blotting was employed to examine protein levels of Cyt *c*, GSDME-FL, and GSDME-N in the cytosol or mitochondria of WT and *Gsdme*$^{-/-}$ 661W photoreceptor cells treated with 5 μM of atRAL for 6 h, respectively. Cells incubated with DMSO alone served as controls. COX IV and GAPDH were used as loading controls. *B*, protein levels of cytosolic Cyt *c* (normalized to GAPDH) ($F_{0.05}$ (1,8) = 29.19, p = 0.0006) and mitochondrial Cyt *c* (normalized to COX IV) ($F_{0.05}$ (1,8) = 7.339, p = 0.0267) were expressed as fold changes compared with DMSO-treated WT controls. Statistical analyses were evaluated by two-way ANOVA with Tukey's post-test. *C*, TEM images of mitochondria in WT or *Gsdme*$^{-/-}$ 661W photoreceptor cells exposed for 6 h to 5 μM of atRAL and DMSO alone, respectively. The scale bars represent 500 nm (*upper panels*) and 200 nm (*lower panels*). atRAL, all-*trans*-retinal; COX IV, cytochrome *c* oxidase, subunit 4; Cyt *c*, cytochrome *c*; DMSO, dimethyl sulfoxide; GSDME-FL, full-length GSDME; GSDME-N, N-terminal fragment of GSDME; TEM, transmission electron microscopy.

necroptosis is impossible to exist in neural retina of light-exposed *Abca4*$^{-/-}$*Rdh8*$^{-/-}$ mice on a C57BL/6J genetic background. However, RIP3 expression was clearly detected in the RPE of C57BL/6J WT mice (Fig. S3).

The most studied executioners of pyroptotic cell death are GSDMD and GSDME (15, 23–27). Our studies found that GSDME-N was significantly present in atRAL-loaded 661W photoreceptor cells, but GSDMD-N was absent (Fig. 3, *E* and *F*), which reveals that photoreceptor pyroptosis caused by atRAL is dependent on GSDME but not GSDMD. Evidence from a previous report has shown that active caspase-3 cleaves GSDME to generate GSDME-N that perforates the plasma membrane for pyroptosis induction (27). Herein, caspase-3 silencing distinctly attenuated the generation of GSDME-N by atRAL in 661W photoreceptor cells, and it effectively rescued cell morphology, protected the plasma membrane, and increased cell survival (Fig. 3, *M*–*Q*), thereby demonstrating that caspase-3 activation is required for GSDME activation leading to photoreceptor pyroptosis.

Interestingly, in addition to reducing pyroptotic cell death, GSDME knockout significantly inhibited cleavage of caspase-3 in 661W photoreceptor cells after atRAL exposure (Fig. 4), implying that GSDME activation is also capable of inducing the production of active caspase-3, which in turn may activate GSDME to aggravate photoreceptor pyroptosis.

A considerable body of research has shown that caspase-3, a caspase protein that acts as a critical executioner of apoptotic cell death, can be activated through the mitochondrial apoptotic signaling pathway in which damage to mitochondrial membrane integrity results in release of Cyt *c* from mitochondria into the cytosol where it promotes caspase-9 and caspase-3 cascade activation (14, 37, 38). We corroborated the presence of mitochondrial GSDME-N and the increase of cytosolic Cyt *c* levels in atRAL-loaded 661W photoreceptor cells (Figs. S2 and 5, *A* and *B*), which discloses that GSDME activation by atRAL may directly disrupt mitochondrial membranes, leading to release of Cyt *c* from mitochondria into the cytosol. However, knocking out GSDME effectively

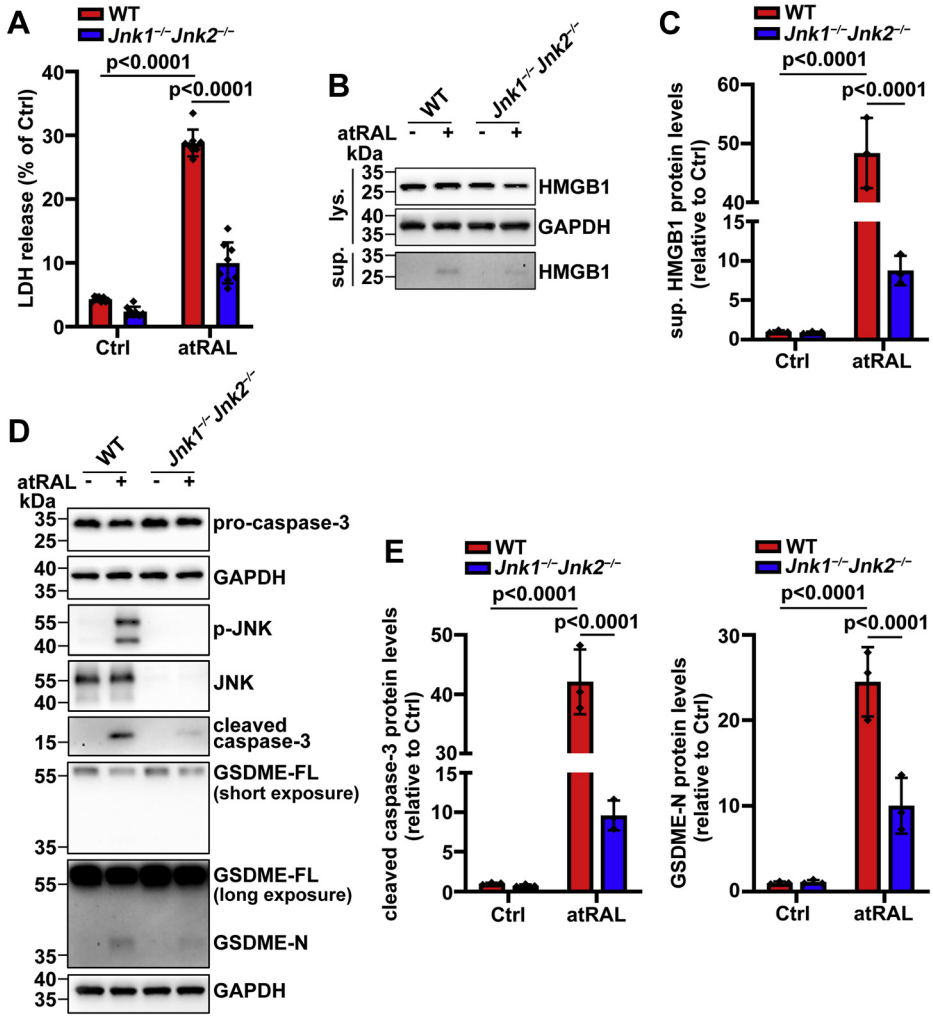

Figure 6. Inactivation of JNK signaling effectively mitigates rupture of the plasma membrane of atRAL-loaded 661W photoreceptor cells through restricting activation of GSDME by caspase-3. *A*, rupture of the plasma membrane was examined by LDH release assay. WT or *Jnk1*$^{-/-}$*Jnk2*$^{-/-}$ 661W photoreceptor cells were treated with 5 μM of atRAL and DMSO alone for 6 h, respectively. $F_{0.05}$ (1,28) = 145.6, $p < 0.0001$. *B* and *C*, Western blot analysis of HMGB1 in cell lysates or culture supernatants from WT or *Jnk1*$^{-/-}$*Jnk2*$^{-/-}$ 661W photoreceptor cells exposed to 5 μM of atRAL and DMSO alone for 6 h, respectively. Protein levels of sup. HMGB1 were normalized to those of GAPDH and presented as fold changes compared with DMSO-treated WT controls. $F_{0.05}$ (1,8) = 119.9, $p < 0.0001$. *D*, Western blotting was used to analyze protein levels of procaspase-3, p-JNK, JNK, cleaved caspase-3, GSDME-FL, and GSDME-N in cell lysates of WT or *Jnk1*$^{-/-}$*Jnk2*$^{-/-}$ 661W photoreceptor cells incubated with 5 μM of atRAL and DMSO alone for 6 h, respectively. *E*, protein levels of cleaved caspase-3 ($F_{0.05}$ (1,8) = 93.16, $p < 0.0001$) and GSDME-N ($F_{0.05}$ (1,8) = 23.61, $p = 0.0013$) were normalized to those of GAPDH and expressed as fold changes compared with DMSO-treated WT controls. Statistical analyses in *A*, *C*, and *E* were determined by two-way ANOVA with Tukey's post-test. atRAL, all-*trans*-retinal; DMSO, dimethyl sulfoxide; GSDME, gasdermin E; GSDME-FL, full-length GSDME; GSDME-N, N-terminal fragment of GSDME; HMGB1, high-mobility group box 1; JNK, c-Jun N-terminal kinase; LDH, lactate dehydrogenase; sup., supernatant.

maintained the integrity of mitochondrial membranes and thereby prevented Cyt *c* release into the cytosol in 661W photoreceptor cells following atRAL exposure, and it significantly rescued mitochondrial morphology (Fig. 5). In addition, deleting GSDME showed a powerful capacity to preclude the release of LDH and HMGB1 from atRAL-loaded 661W photoreceptor cells by exerting a protective effect on the plasma membrane integrity (Fig. 4, *B*, *H*, and *I*), and it clearly protected cellular morphology (Fig. 4*D*). To know how the viability of *Gsdme*$^{-/-}$ 661W photoreceptor cells after 6 h of exposure to 5 μM of atRAL changes over time, the culture medium, after 6 h of treatment of the cells with atRAL, was removed and replaced with fresh Dulbecco's modified Eagle's medium (Gibco) followed by additional incubation for 6 or 12 h. MTS assay results indicated that the viability of *Gsdme*$^{-/-}$ and WT 661W photoreceptor cells incubated for 6 h with 5 μM of atRAL was down by 24.2 and 44.8%, respectively (Fig. S4). After surviving the initial insult, the viability of *Gsdme*$^{-/-}$ 661W photoreceptor cells was reduced by 29.9% at 6 h, and no further decrease in cell viability was observed at 12 h (Fig. S4), suggesting that severely damaged cells will ultimately be eliminated. By contrast, the viability of WT 661W photoreceptor cells was decreased by 33% at 6 h and exhibited a further reduction of 6.8% at 12 h (Fig. S4). However, at each time point, cell viability following exposure to atRAL was significantly elevated in *Gsdme*$^{-/-}$ *versus* WT 661W photoreceptor cells (Fig. S4).

There is already compelling evidence that caspase-3-mediated cleavage of PARP denotes the execution of apoptosis by active caspase-3 (35). Our results showed that

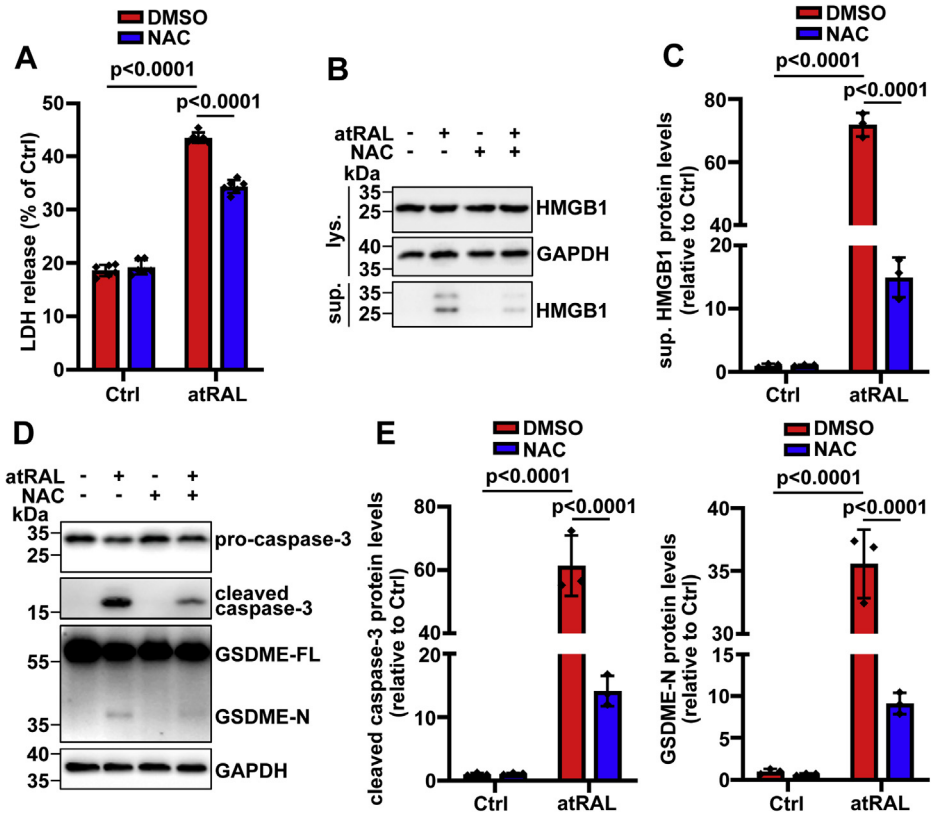

Figure 7. Antioxidant therapy with NAC represses activation of GSDME by caspase-3 to prevent rupture of the plasma membrane of atRAL-loaded 661W photoreceptor cells. *A*, rupture of the plasma membrane was assessed by LDH release assay. 661W photoreceptor cells were incubated with 5 μM of atRAL for 6 h in the presence or the absence of 2 mM of NAC. Note that cells were pretreated with NAC for 2 h. Cells treated with NAC or DMSO alone served as controls. $F_{0.05}$ (1,20) = 103.7, $p < 0.0001$. *B* and *C*, immunoblot analysis of HMGB1 in cell lysates or culture supernatants from 661W photoreceptor cells exposed to 5 μM of atRAL for 6 h with 2 mM of NAC. Note that cells were pretreated with NAC for 2 h. Protein levels of sup. HMGB1 were normalized to those of GAPDH and expressed as fold changes compared with DMSO-treated WT controls. $F_{0.05}$ (1,8) = 399.8, $p < 0.0001$. *D*, 661W photoreceptor cells were preincubated with 2 mM of NAC for 2 h and then treated with 5 μM of atRAL for 6 h. Cell lysates were collected and subjected to Western blot analysis of procaspase-3, cleaved caspase-3, GSDME-FL, and GSDME-N. *E*, protein levels of cleaved caspase-3 ($F_{0.05}$ (1,8) = 69.28, $p < 0.0001$) and GSDME-N ($F_{0.05}$ (1,8) = 223.5, $p < 0.0001$) were normalized to those of GAPDH and expressed as fold changes compared with DMSO-treated WT controls. Statistical analyses in *A*, *C*, and *E* were performed by using two-way ANOVA with Tukey's post-test. atRAL, all-*trans*-retinal; DMSO, dimethyl sulfoxide; GSDME, gasdermin E; GSDME-FL, full-length GSDME; GSDME-N, N-terminal fragment of GSDME; HMGB1, high-mobility group box 1; LDH, lacate dehydrogenase; NAC, *N*-acetyl-L-cysteine; sup., supernatant.

elimination of *Gsdme* gene clearly repressed PARP cleavage in 661W photoreceptor cells in response to atRAL (Fig. 4, *F* and *G*), thus revealing that GSDME activation also stimulates the induction of photoreceptor apoptosis by atRAL *via* enhancing caspase-3 activation.

Considering that GSDME activation required caspase-3 activation in atRAL-loaded 661W photoreceptor cells (Fig. 3, *I*–*Q*), activation of GSDME is likely a secondary event in the course of mitochondrial membrane rupture, and it is responsible for accentuating damage to the mitochondria. We have recently described that activation of JNK signaling by atRAL destroys mitochondria and then results in Cyt *c* release into the cytosol by activating mitochondrial Bak in 661W photoreceptor cells (6). In this study, it was found that complete deletion of JNK signaling dramatically decreased protein levels of GSDME-N and cleaved caspase-3 in 661W photoreceptor cells in response to atRAL, and it significantly sustained the integrity of the plasma membrane (Fig. 6), thereby revealing that JNK activation by atRAL is an important causative factor of mitochondria-mediated caspase-3-dependent activation of GSDME for pyroptosis induction.

Palczewski *et al.* (12) have previously reported that atRAL induces ROS production in photoreceptors through NADPH oxidase. Suppression of ROS by antioxidant NAC distinctly attenuated protein levels of cleaved caspase-3 and GSDME-N in 661W photoreceptor cells after atRAL exposure, and it prevented the rupture of the plasma membrane (Fig. 7), indicative of the involvement of ROS in atRAL-induced photoreceptor pyroptosis. In addition, evidence presented by our laboratory has indicated that treatment with NAC inhibits JNK activation in atRAL-loaded 661W photoreceptor cells through reducing ROS production (6), which in turn implies that ROS overproduction facilitates photoreceptor pyroptosis caused by atRAL at least in part *via* activating JNK signaling.

It should be mentioned here that physiological significance of the atRAL concentration used in this study has been well elucidated (6). In animal studies, we observed a significant induction of GSDME-N, a direct pyroptosis executioner, in photoreceptor ONL of light-exposed *Abca4*$^{-/-}$*Rdh8*$^{-/-}$ mice (Fig. 1*B*). Moreover, genetic inactivation of GSDME visibly attenuated caspase-3 activation and photoreceptor atrophy in neural retina of *Abca4*$^{-/-}$*Rdh8*$^{-/-}$ mice upon exposure to light

(Fig. 1, *D–F*). Therefore, inhibition of GSDME activation may be beneficial to ameliorate retinopathies featured by disrupted atRAL clearance through interference with photoreceptor pyroptosis and apoptosis.

Collectively, our data lent support to the conclusion that activation of GSDME by caspase-3 contributed to atRAL-induced photoreceptor degeneration through inciting pyroptosis and amplifying apoptosis *via* a mitochondrial signaling pathway. A plausible mechanism for it was proposed in Figure 8. atRAL that evades reduction accumulates in photoreceptor cells and then induces ROS generation (6). ROS activates JNK signaling to disrupt mitochondrial membranes and thereby evokes the leakage of Cyt *c* into the cytosol (6). However, it should be pointed out that ROS production is not the only way of JNK activation. Cytosolic Cyt *c* combines with Apaf-1 and caspase-9 to form large protein complexes called apoptosomes, which activate caspase-9 and caspase-3 cascade and thus triggers apoptotic cell death (14). As an alternative, caspase-3 activation cleaves and activates GSDME. GSDME-N forms aggregates and pores in the plasma membrane and then drives pyroptotic cell death. Opening of the plasma membrane during pyroptosis gives rise to the release of intracellular contents, such as HMGB1, to the outside of the cell. Moreover, GSDME-N translocates to the mitochondria where it aggregates and perforates mitochondrial membranes, which in turn accentuates pyroptosis and apoptosis through enhancing Cyt *c* release and caspase-3 activation. In light of current and previous studies, we conclude that photoreceptor damage by atRAL is bound up with apoptosis (6), ferroptosis (7), and pyroptosis but is independent of necroptosis. Because of the identification of GSDME but not GSDMD as an executioner of pyroptosis and an amplifier of apoptosis in photoreceptors suffering from atRAL accumulation, GSDME may be an efficient and promising target for the therapy of photoreceptor degeneration in patients with dry AMD and STGD1.

Experimental procedures

Reagents and antibodies

atRAL, atROL, Hoechst 33342, and 4′,6-diamidino-2-phenylindole were purchased from Sigma–Aldrich. NAC was obtained from Aladdin. Nec-1 was purchased from Selleck. Lipofectamine RNAiMAX reagent and Lipofectamine LTX & PLUS reagent were purchased from Thermo Fisher Scientific. SYTOX Dead Cell Stain Sampler Kit (catalog no.: S34862) was provided by Invitrogen. Antibodies against cleaved caspase-3 (catalog no.: 9664S), PARP (catalog no.: 9542S), p-JNK (catalog no.: 9255S), JNK (catalog no.: 9252S), COX IV (cytochrome *c* oxidase, subunit 4; catalog no.: 4844S), Cyt *c* (catalog no.: 11940S), and GAPDH (catalog no.: 5174S) were provided by

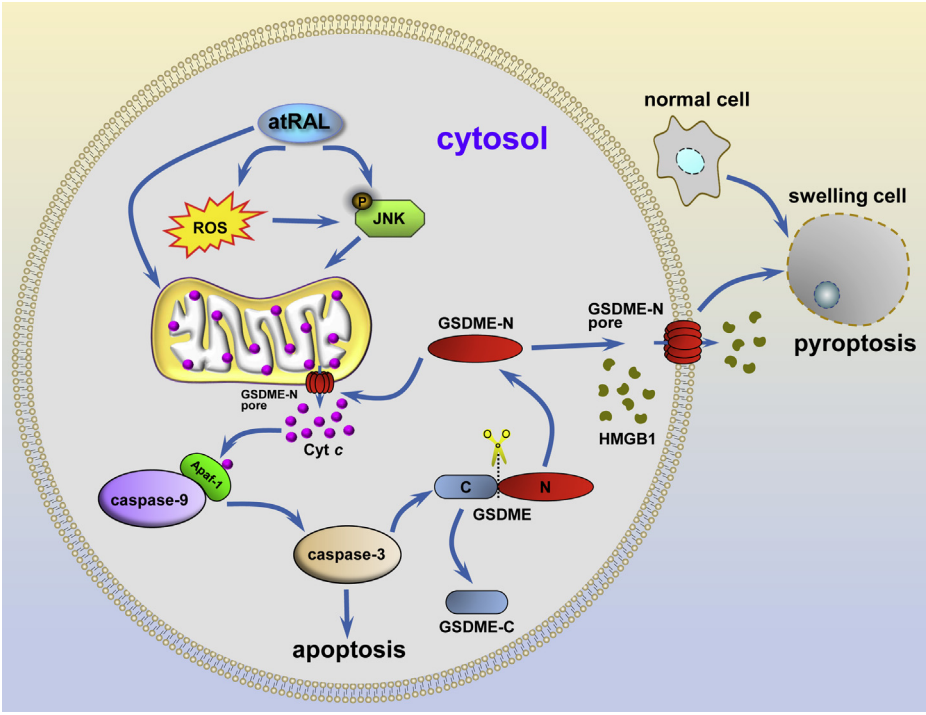

Figure 8. Proposed mechanisms for the induction of photoreceptor cell death by atRAL-mediated activation of GSDME. In photoreceptor cells, atRAL stimulates JNK activation, which is at least partially mediated by ROS production, thereby causing damage to the mitochondria (6). Rupture of the mitochondria releases Cyt *c* into the cytosol, where it promotes the formation of apoptosomes consisting of Cyt *c*, Apaf-1, and caspase-9 (14). Active caspase-9 cleaves and activates caspase-3, leading to caspase-dependent apoptosis. Alternatively, active caspase-3 cleaves GSDME to generate GSDME-N, which forms aggregates and pores in the plasma membrane and then drives pyroptosis. Rupture of the plasma membrane during pyroptosis results in the leakage of intracellular components, such as HMGB1. In addition, GSDME-N moves to the mitochondria, where it aggregates and permeabilizes mitochondrial membranes, thus aggravating pyroptosis and apoptosis by accentuating Cyt *c* release and caspase-3 activation. atRAL, all-*trans*-retinal; Cyt *c*, cytochrome *c*; GSDME, gasdermin E; GSDME-N, N-terminal fragment of GSDME; HMGB1, high-mobility group box 1; JNK, c-Jun N-terminal kinase; ROS, reactive oxygen species.

Cell Signaling Technology. Antibodies against GSDMD (catalog no.: ab209845), GSDME (catalog no.: ab215191), *N*-terminal GSDME (GSDME-N) (catalog no.: ab222407), HMGB1 (catalog no.: ab18256), p-MLKL (catalog no.: ab187091), and rhodopsin (catalog no.: ab3267) were purchased from Abcam. Horseradish peroxidase–conjugated goat anti-rabbit immunoglobulin G (IgG) (H + L) (catalog no.: 31460), Alexa Fluor 594-conjugated donkey anti-rabbit IgG (H + L) (catalog no.: A21207), and antimouse IgG (H + L) (catalog no.: A21203) secondary antibodies were purchased from Thermo Fisher Scientific. PrimeSTAR HS (Premix) (catalog no.: R040A) and pMD 19-T Vector Cloning Kit (catalog no.: 6013) were provided by Takara Biomedical Technology. *Escherichia coli* DH5α was purchased from Transgene Biotech. ReverTra Ace qPCR RT Master Mix was obtained from Toyobo. FastStart Essential DNA Green Master was purchased from Roche. Polyvinylidene fluoride membrane was purchased from Merck Millipore.

Animals

C57BL/6J WT mice were purchased from the Xiamen University Laboratory Animal Center. *Abca4*$^{-/-}$*Rdh8*$^{-/-}$ mice on a C57BL/6J genetic background were generated as we previously described (6). The Jiahuai Han laboratory (School of Life Sciences, Xiamen University) generously provided us with *Gsdme*$^{+/-}$ mice having a genetic background of C57BL/6J. Breeding of *Gsdme*$^{+/-}$ mice produced *Gsdme*$^{-/-}$ mice. *Abca4*$^{-/-}$*Rdh8*$^{-/-}$*Gsdme*$^{-/-}$ mice were obtained by crossing *Abca4*$^{-/-}$*Rdh8*$^{-/-}$ mice with *Gsdme*$^{-/-}$ mice. In comparison with C57BL/6N mice containing the *rd8* mutation in the *Crb1* gene, C57BL/6J WT, *Abca4*$^{-/-}$*Rdh8*$^{-/-}$, *Gsdme*$^{-/-}$, and *Abca4*$^{-/-}$*Rdh8*$^{-/-}$*Gsdme*$^{-/-}$ mice (C57BL/6J genetic backgrounds) did not carry the *rd8* mutation of the *Crb1* gene (Fig. 1*G*). PCR genotyping of the mice with knockouts of *Abca4* and *Rdh8* genes (Fig. 1*G*) was carried out as we previously reported (6). *Gsdme*$^{-/-}$ and *Abca4*$^{-/-}$*Rdh8*$^{-/-}$*Gsdme*$^{-/-}$ mice were further identified by genome sequencing and Western blotting (Fig. 1*G*). Specific primers for amplification of genomic DNAs are shown in Table 1. All procedures involving mice were approved by the Institutional Animal Care and Use Committee of Xiamen University School of Medicine and followed the CARVO statement for the use of animals in ophthalmic and vision research. Mice were housed at the animal care facility of the Xiamen University Laboratory Animal Center under a standard pathogen-free environment with a 12-h light/dark schedule and provided with food and water *ad libitum*. C57BL/6J WT, *Abca4*$^{-/-}$*Rdh8*$^{-/-}$, *Gsdme*$^{-/-}$, and *Abca4*$^{-/-}$*Rdh8*$^{-/-}$*Gsdme*$^{-/-}$ mice at 4 weeks of age were placed in a dark room for 48 h. After pupils of dark-adapted mice were dilated with 1% tropicamide, they were exposed to 10,000 lx light-emitting diode light for 2 h and then kept in the dark for 5 days. The resulting mice were euthanized, and their eyeballs were collected for subsequent studies. Control C57BL/6J WT, *Abca4*$^{-/-}$*Rdh8*$^{-/-}$, *Gsdme*$^{-/-}$, and *Abca4*$^{-/-}$*Rdh8*$^{-/-}$*Gsdme*$^{-/-}$ mice were maintained normally in the dark for 7 days in the absence of light exposure.

Table 1
Primers for genotyping

Primer	Sequences
A0	CCACAGCACACATCAGCATTTCTCC
N1	TGCGAGGCCAGAGGCCACTTGTGTAGC
ABCR1	GCCCAGTGGTCGATCTGTCTAGC
ABCR2	CGGACACAAAGGCCGCTAGGACCACG
Neo1	TGCGAGGCCAGAGGCCACTTGTGTAGC
DMR11	TCCGCCTTGGAAACCTGAGCCAGAAG
DMR5	GAAGGAGCCATTGGAGGCAGCTGC
DMR6	CTGGAAGCACAGCTTTGACCAGAC
mCrb1 mF1	GTGAAGACAGCTACAGTTCTGATC
mCrb1 mF2	GCCCCTGTTTGCATGGAGGAAACTTGGA AGACAGCTACAGTTCTTCTG
mCrb1 mR	GCCCCATTTGCACACTGATGAC
mGsdme-F	GAGGTAGGTAACGATGAGTC
mGsdme-R	GAGTCCACTTCTCCATCTG

H&E staining

Mouse eyeballs were fixed in 4% paraformaldehyde at 4 °C overnight and then embedded in paraffin. H&E staining of paraffin-embedded tissue sections at a thickness of 8 μm was conducted as previously described (6).

Cell culture

661W photoreceptor cells were routinely maintained as previously reported (6).

Treatment with atRAL and atROL

661W photoreceptor cells seeded into 96-well plates (1.5 × 10^4 cells per well) or 6-well plates (3 × 10^5 cells per well) were cultured overnight, followed by incubation with 5 μM of atRAL or 5, 10, and 20 μM of atROL for 6 h. Alternatively, the cells seeded into 10 cm dishes, 6 h after incubation with 5 μM atRAL or atROL, were thoroughly washed with PBS to ensure that only intracellular atRAL or atROL remained. Cellular extracts were subjected to HPLC analysis.

Treatment with NAC or Nec-1

661W photoreceptor cells were pretreated with 2 mM of NAC for 2 h or 50 of μM Nec-1 for 1 h and then incubated with 5 μM of atRAL for 6 h.

Plasmid transfection

pEGFP-C1-mRDH8, purchased from Sangon Biotech Co, Ltd, was prepared by insertion of the FL mouse RDH8 complementary DNA (cDNA) fused with an N-terminal GFP into vector pEGFP-C1. 661W photoreceptor cells were transfected with pEGFP-C1-mRDH8 or control vector pEGFP-C1 using Lipofectamine LTX & PLUS reagent according to the manufacturer's protocol. About 24 h post-transfection, cells were treated with 5 μM of atRAL for 6 h. Cell lysates were examined using Western blotting. Cellular extracts were analyzed by reverse-phase HPLC.

HPLC analysis

Cell pellets were extracted as described previously (39). The resulting extract was dissolved in 100 μl of methanol. After

Table 2
Guide RNA sequences

Gene	Forward primer	Reverse primer
Gsdme	CACCGACCATAAGAGCG GGGCTATT	AAACAATAGCCCCGCT CTTATGGTC

centrifugation at 10,000*g* for 5 min, the supernatant was injected into reverse-phase HPLC using an Alliance System (Waters Corp) equipped with a 2695 separation module and a 2998 photodiode array detector. Compounds were separated on a Waters Atlantis dC18 reverse-phase column (3 μm, 4.6 × 150 mm) with a gradient mobile phase consisting of acetonitrile and water in the presence of 0.1% trifluoroacetic acid (85–100% acetonitrile, 0.8 ml/min, 15 min). The peak area (microvolts per second) was integrated using Empower version 3 software. Photodiode array detection was set at 380 nm for atRAL and 325 nm for atROL.

Generation of knockout cell lines using CRISPR–Cas9

Jnk1$^{-/-}$*Jnk2*$^{-/-}$ 661W photoreceptor cell line was prepared as we previously described (6). By contrast, a target sequence in the second exon of mouse *Gsdme* (ACCATAAGAG CGGGGCTATT) was designed at Massachusetts Institute of Technology (http://crispr.mit.edu). The oligonucleotides for specific guide RNAs were presented in Table 2 and synthesized by Sangon Biotech. The guide RNAs were cloned into the BsmbI site of pL-CRISPR.EFS.GFP vector purchased from Addgene. The targeting vector was transfected into 661W photoreceptor cells seeded into 6-well plates (2 × 10^5 cells per well) using the Lipofectamine LTX & PLUS reagent according to the manufacturer's instruction. About 24 h post-transfection, GFP-positive live cells were sorted into single clones using a MoFlo Astrios Flow Cytometry (Beckman Coulter). Single cells were cultured in 96-well plates for at least 2 weeks. *Gsdme*$^{-/-}$ 661W photoreceptor cells were identified by Western blotting and DNA sequencing. The primers for amplification of the genomic areas designed for *Gsdme* are shown in Table 3. WT, *Jnk1*$^{-/-}$*Jnk2*$^{-/-}$, or *Gsdme*$^{-/-}$ 661W photoreceptor cells seeded into 96-well or 6-well plates were cultured overnight and then incubated with 5 μM of atRAL for 6 h.

RNA interference

The mouse-specific siRNA targeting caspase-3 was designed and synthesized by GenePharma (Table 4). 661W photoreceptor cells seeded into 96-well plates (0.6 × 10^4 cells per well) or 6-well plates (1.2 × 10^5 cells per well) were cultured overnight. Transfection of caspase-3-targeting siRNA into cells was performed using the Lipofectamine RNAiMAX reagent according to the manufacturer's protocol. At 24 h post-transfection, the cells were treated with 5 μM of atRAL for 6 h. The knockdown efficiency of caspase-3 was examined by qRT–PCR and Western blotting.

Table 3
Primers for amplification of genomic DNA

Gene	Forward primer	Reverse primer
Gsdme	CTGCCCATGACAACTGAGGT	ATCCACCAGCCTTTCAGCAG

Table 4
siRNA sequences

Gene	Forward primer	Reverse primer
Negative control	UUCUCCGAACGUGU CACGUTT	ACGUGACACGUUCGG AGAATT
Caspase-3	GCUGACUUCCUGUA UGCUUTT	AAGCAUACAGGAAGU CAGCTT

qRT–PCR

Total RNA was isolated from cultured siNC–siCaspase-3-transfected 661W photoreceptor cells using TRIeasy total RNA extraction reagent and reverse transcribed into cDNA utilizing the ReverTra Ace qPCR RT Master Mix. The cDNA was analyzed by qRT–PCR with the FastStart Essential DNA Green Master in a LightCycler 96 instrument (Roche). The qRT–PCR data were shown as normalized ratios calculated using $\Delta\Delta C_T$ method by a Roche LightCycler system. Primer sequences are available in Table 5.

Cell morphology

661W photoreceptor cells seeded into 96-well plates (1.5 × 10^4 cells per well) were cultured overnight and then incubated with 5 μM of atRAL for 6 h. siNC or siCaspase-3 transfected 661W photoreceptor cells were treated for 6 h with 5 μM of atRAL. Images were taken using a Leica DM2500 microscope. Alternatively, WT or *Gsdme*$^{-/-}$ 661W photoreceptor cells seeded into 35 mm cover glass-bottom culture dishes (1.5 × 10^5 cells per well) were cultured overnight, followed by incubation with 5 μM of atRAL for 6 h. Photographs were captured under a Zeiss LSM 880 + Airyscan confocal microscope.

Cell viability

MTS assay for evaluating cellular survival was performed as previously reported (6).

LDH release assay

Plasma membrane damage was evaluated by measuring the release of LDH into culture supernatants with an LDH cytotoxicity assay kit (Yeasen). The absorbance at a wavelength of 490 nm was recorded in a Multiskan GO-1510 spectrophotometer (Thermo Fisher Scientific). LDH release was expressed as a percentage of total (supernatant plus cellular) LDH.

Table 5
Primer sequences

Gene	Forward primer	Reverse primer
Caspase-3	GCTTGGAACGGTAC GCTAAG	GAGTCCACTGACTT GCTCCC
β-actin	GATCAAGATCATTGC TCCTCCTG	AGGGTGTAAAACGC AGCTCA

SYTOX Orange staining

WT and *Gsdme*$^{-/-}$ 661W photoreceptor cells seeded into 6-well plates (3 × 10^5 cells per well) were cultured overnight. Cells were treated with 5 μM of atRAL for 6 h and then stained with Hoechst 33342 and SYTOX Orange dead cell stain (250 nM) for 20 min at 37 °C in the dark. After being washed by PBS three times, fluorescence micrographs were taken using the Leica DM2500 microscope.

TEM

TEM analysis of mitochondrial ultrastructures in WT or *Gsdme*$^{-/-}$ 661W photoreceptor cells incubated with 5 μM of atRAL for 6 h was performed as previously described (7).

Immunostaining

Mouse eyeballs were fixed in 4% paraformaldehyde at 4 °C overnight and embedded in paraffin. After dried at 60 °C for 1 h, paraffin sections of 6 μm were deparaffinized and immersed in citrate antigen retrieval solution (3 g/l trisodium citrate dihydrate and 0.4 g/l citric acid; pH 6.0, 100 °C). About 30 min later, the sections were moved out and allowed to cool to room temperature. Subsequently, they were blocked by 2% bovine serum albumin for 2 h at room temperature and immediately incubated with primary antibodies (1:100 dilution) overnight at 4 °C, followed by incubation with Alexa Fluor 594-conjugated secondary antibodies (1:200 dilution) for 1 h at room temperature in the dark. Unbound secondary antibodies were washed off with PBS, and then the sections were counterstained with 4′,6-diamidino-2-phenylindole to mark nuclei (*blue*). Immunostaining images were viewed and photographed on an Olympus FV1000 confocal microscope.

Western blotting

Cells were incubated on ice with radioimmunoprecipitation assay lysis buffer containing protease and phosphatase inhibitor cocktail (Thermo Fisher Scientific) for 30 min. The lysates were clarified by centrifugation at 10,000*g* for 10 min at 4 °C, and protein concentration was quantified by the Bicinchoninic Acid Protein Assay Kit (Thermo Fisher Scientific). Equal amounts of proteins in each sample were separated on 12% SDS-PAGE gels and transferred onto polyvinylidene fluoride membranes. The membranes were blocked with 5% (w/v) skim milk in Tris-buffered saline (pH 7.4) containing 1% Tween-20 for 2 h at room temperature and probed with primary antibodies (1:1000 dilution) at 4 °C overnight. After being washed three times in Tris-buffered saline (pH 7.4) containing 1% Tween-20, the membranes were incubated with secondary antibodies conjugated to horseradish peroxidase (1:5000 dilution) for 2 h at room temperature. The signals were detected by the ChemiDoc XRS+ imaging system (Bio-Rad) after incubating the membranes with ECL Western Blotting Detection Reagents (Advansta). Alternatively, cell culture supernatants were precipitated by the addition of an equal volume of methanol and 0.25 volumes of chloroform to each sample, followed by centrifugation at 10,000*g* for 15 min at 4 °C. After discarding the upper and lower phases, 500 μl of methanol was added to the interphase of each sample and then centrifuged at 10,000*g* for 15 min at 4 °C. For Western blot analysis, the pellets were dried at 4 °C, resuspended in protein loading buffer, and boiled at 100 °C for 5 min. Unprocessed original images of gels, in which boxes in *red* indicated selected Western blot results, were presented in Fig. S5.

Isolation of cytosolic and mitochondrial fractions

WT and *Gsdme*$^{-/-}$ 661W photoreceptor cells were incubated with 5 μM of atRAL for 6 h, respectively. Cytosolic and mitochondrial fractions of cells were isolated as described previously (6). The supernatants were collected as the cytosolic fraction. The pellets were resuspended in Triton lysis buffer (25 mM Tris–HCl [pH 8.0], 0.1% [v/v] Triton X-100, and protease inhibitors) and incubated on ice for 10 min. After being centrifuged at 10,000*g* at 4 °C for 10 min, the supernatants were gained as the mitochondrial fraction. Immunoblotting was used to analyze protein levels of Cyt *c*, GSDME-FL, and GSDME-N in the cytosol and mitochondria, respectively.

Statistical analyses

Data were expressed as mean ± SD of at least three independent experiments. Statistical analyses were conducted by Student's *t* test and one-way or two-way ANOVA with Tukey's post-test using GraphPad Prism software (version 8.0; Graph Pad Software, Inc), as shown in the corresponding legends to the figures. Differences were considered significant at a p value of less than 0.05.

Data availability

The data supporting the findings of this study are available within the article and the supporting information.

Supporting information—This article contains supporting information.

Author contributions—Y. W. conceptualization; B. C. and Y. W. formal analysis; B. C., C. L., D. H., J. C., J. L., K. Q., W. L., X. W., and Y. W. investigation; J. H. resources; B. C. and Y. W. writing–original draft; Z. L. and Y. W. writing–review and editing; Y. W. supervision; Y. W. project administration; Y. W. funding acquisition.

Funding and additional information—This work was supported in part by grants from China National Natural Science Foundation (grant nos.: 82171064 and 81870671 to Y. W.), Guangdong Basic and Applied Basic Research Foundation (grant no.: 2021A1515011391 to Y. W.), the Basic Research Program of Shenzhen (grant no.: JCYJ20180306173025004 to Y. W.), and XMU Training Program of Innovation and Entrepreneurship for Undergraduates.

Conflict of interest—The authors declare that they have no conflicts of interest with the contents of this article.

Abbreviations—The abbreviations used are: ABCA4, ABC (subfamily A, member 4) transporter; AMD, age-related macular

degeneration; atRAL, all-*trans*-retinal; atROL, all-*trans*-retinol; cDNA, complementary DNA; Cyt *c*, cytochrome *c*; GSDME, gasdermin E; GSDME-N, N-terminal fragment of GSDME; HMGB1, high-mobility group box 1; IgG, immunoglobulin G; IS, inner segment; JNK, c-Jun N-terminal kinase; LDH, lactate dehydrogenase; NAC, *N*-acetyl-L-cysteine; Nec-1, necrostatin-1; ONL, outer nuclear layer; OS, outer segment; PARP, poly-ADP-ribose polymerase; PCD, programmed cell death; p-MLKL, phosphorylated mixed lineage kinase domain-like protein; qRT–PCR, quantitative real-time PCR; RDH8, all-*trans*-retinol dehydrogenase 8; RIP3, receptor interacting protein kinase 3; ROS, reactive oxygen species; RPE, retinal pigment epithelium; STGD1, Stargardt's disease 1; TEM, transmission electron microscopy.

References

1. Kiser, P. D., Golczack, M., and Palczewski, K. (2014) Chemistry of the retinoid (visual) cycle. *Chem. Rev.* **114**, 194–232
2. Liu, X., Chen, J., Liu, Z., Li, J., Yao, K., and Wu, Y. (2016) Potential therapeutic agents against retinal diseases caused by aberrant metabolism of retinoids. *Invest. Ophthalmol. Vis. Sci.* **57**, 1017–1030
3. Saari, J. C. (2012) Vitamin A metabolism in rod and cone visual cycles. *Annu. Rev. Nutr.* **32**, 125–145
4. Kiser, P. D., and Palczewski, K. (2016) Retinoids and retinal diseases. *Annu. Rev. Vis. Sci.* **2**, 197–234
5. Maeda, A., Maeda, T., Golczak, M., and Palczewski, K. (2008) Retinopathy in mice induced by disrupted all-*trans*-retinal clearance. *J. Biol. Chem.* **283**, 26684–26693
6. Liao, C., Cai, B., Feng, Y., Chen, J., Wu, Y., Zhuang, J., Liu, Z., and Wu, Y. (2020) Activation of JNK signaling promotes all-*trans*-retinal-induced photoreceptor apoptosis in mice. *J. Biol. Chem.* **295**, 6958–6971
7. Chen, C., Chen, J., Wang, Y., Liu, Z., and Wu, Y. (2021) Ferroptosis drives photoreceptor degeneration in mice with defects in all-*trans*-retinal clearance. *J. Biol. Chem.* **296**, 100187
8. Weng, J., Mata, N. L., Azarian, S. M., Tzekov, R. T., Birch, D. G., and Travis, G. H. (1999) Insights into the function of Rim protein in photoreceptors and etiology of Stargardt's disease from the phenotype in abcr knockout mice. *Cell* **98**, 13–23
9. Quazi, F., Lenevich, S., and Molday, R. S. (2012) ABCA4 is an *N*-retinylidene-phosphatidylethanolamine and phosphatidylethanolamine importer. *Nat. Commun.* **3**, 925
10. Chen, C., Thompson, D. A., and Koutalos, Y. (2012) Reduction of all-*trans*-retinal in vertebrate rod photoreceptors requires the combined action of RDH8 and RDH12. *J. Biol. Chem.* **287**, 24662–24670
11. Maeda, A., Maeda, T., Golczak, M., Chou, S., Desai, A., Hoppel, C. L., Matsuyama, S., and Palczewski, K. (2009) Involvement of all-*trans*-retinal in acute light-induced retinopathy of mice. *J. Biol. Chem.* **284**, 15173–15183
12. Chen, Y., Okano, K., Maeda, T., Chauhan, V., Golczak, M., Maeda, A., and Palczewski, K. (2012) Mechanism of all-*trans*-retinal toxicity with implications for Stargardt disease and age-related macular degeneration. *J. Biol. Chem.* **287**, 5059–5069
13. Dixon, S. J., Lemberg, K. M., Lamprecht, M. R., Skouta, R., Zaitsev, E. M., Gleason, C. E., Patel, D. N., Bauer, A. J., Cantley, A. M., Yang, W. S., Morrison, B., and Stockwell, B. R. (2012) Ferroptosis: An iron-dependent form of nonapoptotic cell death. *Cell* **149**, 1060–1072
14. Green, D. R. (2019) The coming decade of cell death research: Five riddles. *Cell* **177**, 1094–1107
15. Shi, J., Zhao, Y., Wang, K., Shi, X., Wang, Y., Huang, H., Zhuang, Y., Cai, T., Wang, F., and Shao, F. (2015) Cleavage of GSDMD by inflammatory caspases determines pyroptotic cell death. *Nature* **526**, 660–665
16. Ding, J., Wang, K., Liu, W., She, Y., Sun, Q., Shi, J., Sun, H., Wang, D. C., and Shao, F. (2016) Pore-forming activity and structural autoinhibition of the gasdermin family. *Nature* **535**, 111–116
17. Shi, J., Gao, W., and Shao, F. (2017) Pyroptosis: Gasdermin-mediated programmed necrotic cell death. *Trends Biochem. Sci.* **42**, 245–254
18. Erkes, D. A., Cai, W., Sanchez, I. M., Purwin, T. J., Rogers, C., Field, C. O., Berger, A. C., Hartsough, E. J., Rodeck, U., Alnemri, E. S., and Aplin, A. E. (2020) Mutant BRAF and MEK inhibitors regulate the tumor immune microenvironment via pyroptosis. *Cancer Discov.* **10**, 254–269
19. Hou, J., Zhao, R., Xia, W., Chang, C. W., You, Y., Hsu, J. M., Nie, L., Chen, Y., Wang, Y. C., Liu, C., Wang, W. J., Wu, Y., Ke, B., Hsu, J. L., Huang, K., *et al.* (2020) PD-L1-mediated gasdermin C expression switches apoptosis to pyroptosis in cancer cells and facilitates tumour necrosis. *Nat. Cell Biol.* **22**, 1264–1275
20. Zhou, Z., He, H., Wang, K., Shi, X., Wang, Y., Su, Y., Wang, Y., Li, D., Liu, W., Zhang, Y., Shen, L., Han, W., Shen, L., Ding, J., and Shao, F. (2020) Granzyme A from cytotoxic lymphocytes cleaves GSDMB to trigger pyroptosis in target cells. *Science* **368**, eaaz7548
21. Broz, P., Pelegrín, P., and Shao, F. (2020) The gasdermins, a protein family executing cell death and inflammation. *Nat. Rev. Immunol.* **20**, 143–157
22. Orning, P., Lien, E., and Fitzgerald, K. A. (2019) Gasdermins and their role in immunity and inflammation. *J. Exp. Med.* **216**, 2453–2465
23. Shi, J., Zhao, Y., Wang, Y., Gao, W., Ding, J., Li, P., Hu, L., and Shao, F. (2014) Inflammatory caspases are innate immune receptors for intracellular LPS. *Nature* **514**, 187–192
24. Kayagaki, N., Stowe, I. B., Lee, B. L., O'Rourke, K., Anderson, K., Warming, S., Cuellar, T., Haley, B., Roose-Girma, M., Phung, Q. T., Liu, P. S., Lill, J. R., Li, H., Wu, J., Kummerfeld, S., *et al.* (2015) Caspase-11 cleaves gasdermin D for non-canonical inflammasome signalling. *Nature* **526**, 666–671
25. Liu, X., Zhang, Z., Ruan, J., Pan, Y., Magupalli, V. G., Wu, H., and Lieberman, J. (2016) Inflammasome-activated gasdermin D causes pyroptosis by forming membrane pores. *Nature* **535**, 153–158
26. He, W. T., Wan, H., Hu, L., Chen, P., Wang, X., Huang, Z., Yang, Z. H., Zhong, C. Q., and Han, J. (2015) Gasdermin D is an executor of pyroptosis and required for interleukin-1β secretion. *Cell Res.* **25**, 1285–1298
27. Wang, Y., Gao, W., Shi, X., Ding, J., Liu, W., He, H., Wang, K., and Shao, F. (2017) Chemotherapy drugs induce pyroptosis through caspase-3 cleavage of a gasdermin. *Nature* **547**, 99–103
28. Chen, X., Li, W., Ren, J., Huang, D., He, W. T., Song, Y., Yang, C., Li, W., Zheng, X., Chen, P., and Han, J. (2014) Translocation of mixed lineage kinase domain-like protein to plasma membrane leads to necrotic cell death. *Cell Res.* **24**, 105–121
29. Cai, Z., Jitkaew, S., Zhao, J., Chiang, H. C., Choksi, S., Liu, J., Ward, Y., Wu, L. G., and Liu, Z. G. (2014) Plasma membrane translocation of trimerized MLKL protein is required for TNF-induced necroptosis. *Nat. Cell Biol.* **16**, 55–65
30. Tan, E., Ding, X. Q., Saadi, A., Agarwal, N., Naash, M. I., and Al-Ubaidi, M. R. (2004) Expression of cone-photoreceptor-specific antigens in a cell line derived from retinal tumors in transgenic mice. *Invest. Ophthalmol. Vis. Sci.* **45**, 764–768
31. Li, J., Zhang, Y., Cai, X., Xia, Q., Chen, J., Liao, Y., Liu, Z., and Wu, Y. (2016) All-*trans*-retinal dimer formation alleviates the cytotoxicity of all-*trans*-retinal in human retinal pigment epithelial cells. *Toxicology* **371**, 41–48
32. Wallach, D., Kang, T. B., Dillon, C. P., and Green, D. R. (2016) Programmed necrosis in inflammation: Toward identification of the effector molecules. *Science* **352**, aaf2154
33. Jiang, M., Qi, L., Li, L., and Li, Y. (2020) The caspase-3/GSDME signal pathway as a switch between apoptosis and pyroptosis in cancer. *Cell Death Discov.* **6**, 112
34. Rogers, C., Erkes, D. A., Nardone, A., Aplin, A. E., Fernandes-Alnemri, T., and Alnemri, E. S. (2019) Gasdermin pores permeabilize mitochondria to augment caspase-3 activation during apoptosis and inflammasome activation. *Nat. Commun.* **10**, 1689
35. Tewari, M., Quan, L. T., O'Rourke, K., Desnoyers, S., Zeng, Z., Beidler, D. R., Poirier, G. G., Salvesen, G. S., and Dixit, V. M. (1995) Yama/CPP32 beta, a mammalian homolog of CED-3, is a CrmA-inhibitable protease

that cleaves the death substrate poly(ADP-ribose) polymerase. *Cell* **81**, 801–809
36. Wang, H., Sun, L., Su, L., Rizo, J., Liu, L., Wang, L. F., Wang, F. S., and Wang, X. (2014) Mixed lineage kinase domain-like protein MLKL causes necrotic membrane disruption upon phosphorylation by RIP3. *Mol. Cell* **54**, 133–146
37. Nagata, S. (2018) Apoptosis and clearance of apoptotic cells. *Annu. Rev. Immunol.* **36**, 489–517
38. Kesavardhana, S., Malireddi, R. K., and Kanneganti, T. D. (2020) Caspases in cell death, inflammation, and pyroptosis. *Annu. Rev. Immunol.* **38**, 567–595
39. Gao, Z., Liao, Y., Chen, C., Liao, C., He, D., Chen, J., Ma, J., Liu, Z., and Wu, Y. (2018) Conversion of all-*trans*-retinal into all-*trans*-retinal dimer reflects an alternative metabolic/antidotal pathway of all-*trans*-retinal in the retina. *J. Biol. Chem.* **293**, 14507–14519